Towards robust prediction of the dynamics of the Antarctic ice sheet

Uncertainty quantification of sea-level rise projections and grounding-line retreat with essential ice-sheet models

Kevin Bulthuis[1,2]

[1] Computational and Stochastic Modeling, Université de Liège, Belgium
[2]Laboratory of Glaciology, Université Libre de Bruxelles, Belgium

Motivation: Robust sea-level rise projections

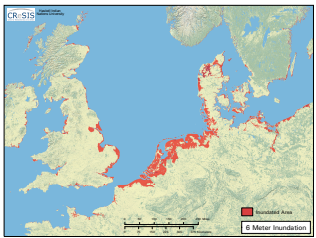

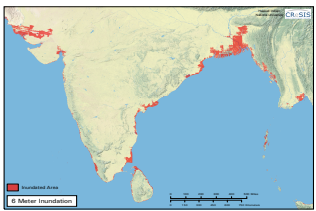

6-m Inundation maps [CreSIS, 2019]

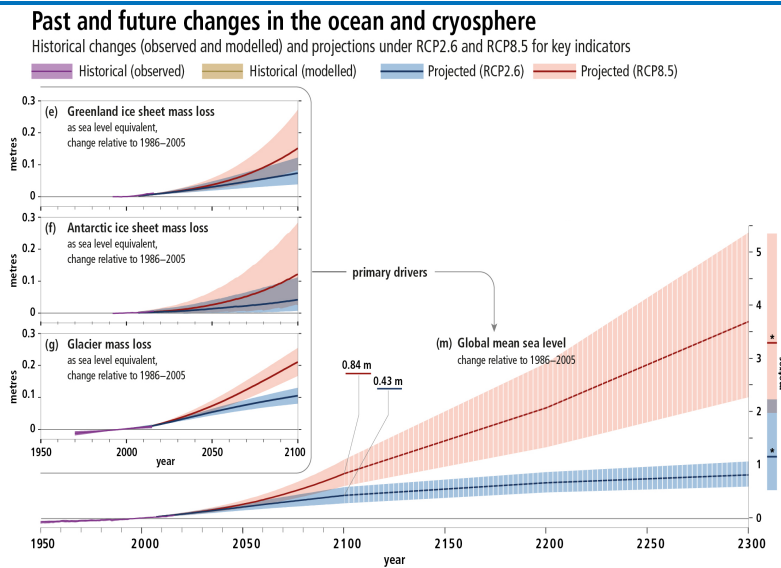

SROCC: Special Report on the Ocean and Cryosphere in a Changing Climat [IPCC, 2019]

Motivation: Marine ice sheets and instabilities

- A substantial fraction of the Antarctic ice sheet rests on a bedrock hundreds of metres below sea level (marine ice sheets) e.g. in West Antarctica and the Wilkes and Aurora basins.
- The net mass loss of the Antarctic ice sheet in a changing climate will be governed by the response of its marine sectors.
- Risk for collapse of marine sectors (especially in West Antarctica) due to marine ice-sheet instability (MISI) and other instability mechanisms (potential risk for a tipping point).

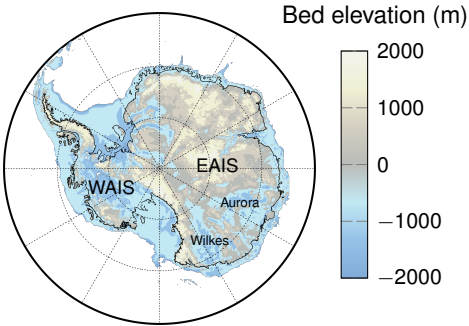

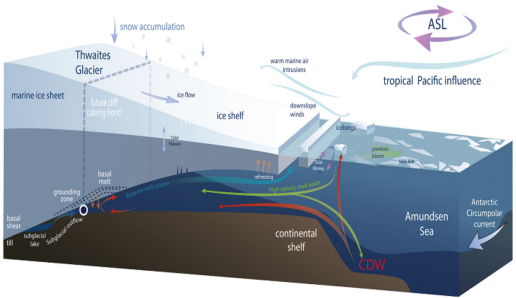

Ice-sheet models and uncertainty quantification (UQ)

- Uncertainty in ice-sheet models:
  - Model uncertainties: Discrepancies with the real-world system;
  - Input uncertainties: uncertain input parameters, initial and boundary conditions, and forcing.
- Since AR5: New generation of ice-sheet models that are amenable to continental simulations of the Antarctic ice sheet (with sufficient accuracy) $\Rightarrow$ New sea-level rise projections e.g. Ritz et al. (2015), Golledge et al. (2015), and DeConto and Pollard (2016).
- Limited insight into the impact of uncertainty in ice-sheet models:
  - Ritz et al. (2015): Probabilistic sea-level rise projections using a statistical approach for the probability of MISI onset.
  - Golledge et al. (2015): Simulations with and without sub-grid melt interpolation. Qualitative insight into the sensitivity of the AIS to temperature, precipitation, and sea-surface temperature.
  - DeConto and Pollard (2016): Assessment of the impact of parametric uncertainty based on a few samples in the parameter space.
- New computationally efficient ice-sheet models for large-scale and long-term simulations and large-ensemble analysis (e.g. f.ETISh) $\Rightarrow$ Opportunities for UQ in ice-sheet modelling.

C. Ritz et al. Potential sea-level rise from Antarctic ice-sheet instability constrained by observations. *Nature*, 2015.
N. R. Golledge. The multi-millennial Antarctic commitment to future sea-level rise. *Nature*, 2015.
R. M. DeConto and D. Pollard. Contribution of Antarctica to past and future sea-level rise. *Nature*, 2016.

Thesis: Contributions

Towards robust prediction of the dynamics of the Antarctic ice sheet: Uncertainty quantification of sea-level rise projections and grounding-line retreat with essential ice-sheet models.

Thesis: Contributions

Towards robust prediction of the dynamics of the Antarctic ice sheet: Uncertainty quantification of sea-level rise projections and grounding-line retreat with essential ice-sheet models.

- In UQ, methods exist to describe quantitatively the origin, propagation, and interplay of sources of uncertainty in the analysis and projection of the behaviour of complex systems.

  $\Rightarrow$ Methods of interest to be applied to the quantification of the impact of uncertain input parameters on a (scalar-valued) quantity of interest of a computational ice-sheet model.

Thesis: Contributions

Towards robust prediction of the dynamics of the Antarctic ice sheet: Uncertainty quantification of sea-level rise projections and grounding-line retreat with essential ice-sheet models.

- In UQ, methods exist to describe quantitatively the origin, propagation, and interplay of sources of uncertainty in the analysis and projection of the behaviour of complex systems.

  $\Rightarrow$ Methods of interest to be applied to the quantification of the impact of uncertain input parameters on a (scalar-valued) quantity of interest of a computational ice-sheet model.

  This thesis: New assessment and new understanding of the impact of uncertainties on the multicentennial response of the Antarctic ice sheet.

Thesis: Contributions

Towards robust prediction of the dynamics of the Antarctic ice sheet: Uncertainty quantification of sea-level rise projections and grounding-line retreat with essential ice-sheet models.

- In UQ, methods exist to describe quantitatively the origin, propagation, and interplay of sources of uncertainty in the analysis and projection of the behaviour of complex systems.

  $\Rightarrow$ Methods of interest to be applied to the quantification of the impact of uncertain input parameters on a (scalar-valued) quantity of interest of a computational ice-sheet model.

  This thesis: New assessment and new understanding of the impact of uncertainties on the multicentennial response of the Antarctic ice sheet.

- Theory and methods needed for UQ of geometrical characteristics of the spatial and temporal response of physics-based computational models.

  $\Rightarrow$ Challenges: probabilistic characterisation of random excursion sets, computational cost, discretisations of spatial and stochastic dimensions.

Thesis: Contributions

Towards robust prediction of the dynamics of the Antarctic ice sheet: Uncertainty quantification of sea-level rise projections and grounding-line retreat with essential ice-sheet models.

- In UQ, methods exist to describe quantitatively the origin, propagation, and interplay of sources of uncertainty in the analysis and projection of the behaviour of complex systems.

  $\Rightarrow$ Methods of interest to be applied to the quantification of the impact of uncertain input parameters on a (scalar-valued) quantity of interest of a computational ice-sheet model.

  This thesis: New assessment and new understanding of the impact of uncertainties on the multicentennial response of the Antarctic ice sheet.

- Theory and methods needed for UQ of geometrical characteristics of the spatial and temporal response of physics-based computational models.

  $\Rightarrow$ Challenges: probabilistic characterisation of random excursion sets, computational cost, discretisations of spatial and stochastic dimensions.

  This thesis: New methods for uncertainty quantification of geometrical characteristics of the spatial response of physics-based computational models.

Thesis: Contributions

Towards robust prediction of the dynamics of the Antarctic ice sheet: Uncertainty quantification of sea-level rise projections and grounding-line retreat with essential ice-sheet models.

- In UQ, methods exist to describe quantitatively the origin, propagation, and interplay of sources of uncertainty in the analysis and projection of the behaviour of complex systems.

  $\Rightarrow$ Methods of interest to be applied to the quantification of the impact of uncertain input parameters on a (scalar-valued) quantity of interest of a computational ice-sheet model.

  This thesis: New assessment and new understanding of the impact of uncertainties on the multicentennial response of the Antarctic ice sheet.

- Theory and methods needed for UQ of geometrical characteristics of the spatial and temporal response of physics-based computational models.

  $\Rightarrow$ Challenges: probabilistic characterisation of random excursion sets, computational cost, discretisations of spatial and stochastic dimensions.

  This thesis: New methods for uncertainty quantification of geometrical characteristics of the spatial response of physics-based computational models.

- Essential ice-sheet models: Efficient for large-scale and long-term simulations and large-ensemble simulations.

Outline

- Introduction
- Outline
- Background:
  - Physics of ice sheets
  - The f.ETISh ice-sheet model
  - Overview of uncertainty quantification methods
- Multifidelity estimation of confidence sets of random excursion sets
- Uncertainty Quantification: Application to Ice-Sheet Modelling:
  - Uncertainty quantification of the multi-centennial response of the Antarctic ice sheet
  - Multi-model comparison of sea-level rise projections
- Conclusion and outlook

Physics of ice sheets

K. M. Cuffey and W. S. B. Paterson. *The Physics of Glaciers*. Butterworth-Heinemann, 2010.
R. Greve and H. Blatter. *Dynamics of Ice Sheets and Glaciers*. Springer, 2009.

Marine ice-sheet dynamics: Full-order model

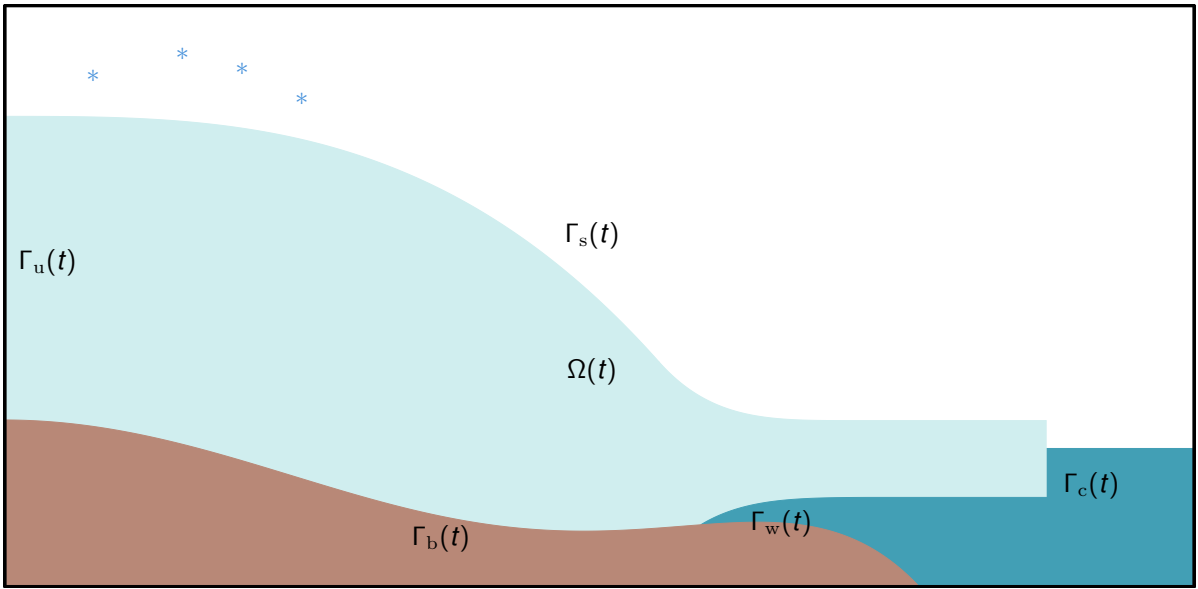

Marine ice-sheet dynamics: Full-order model

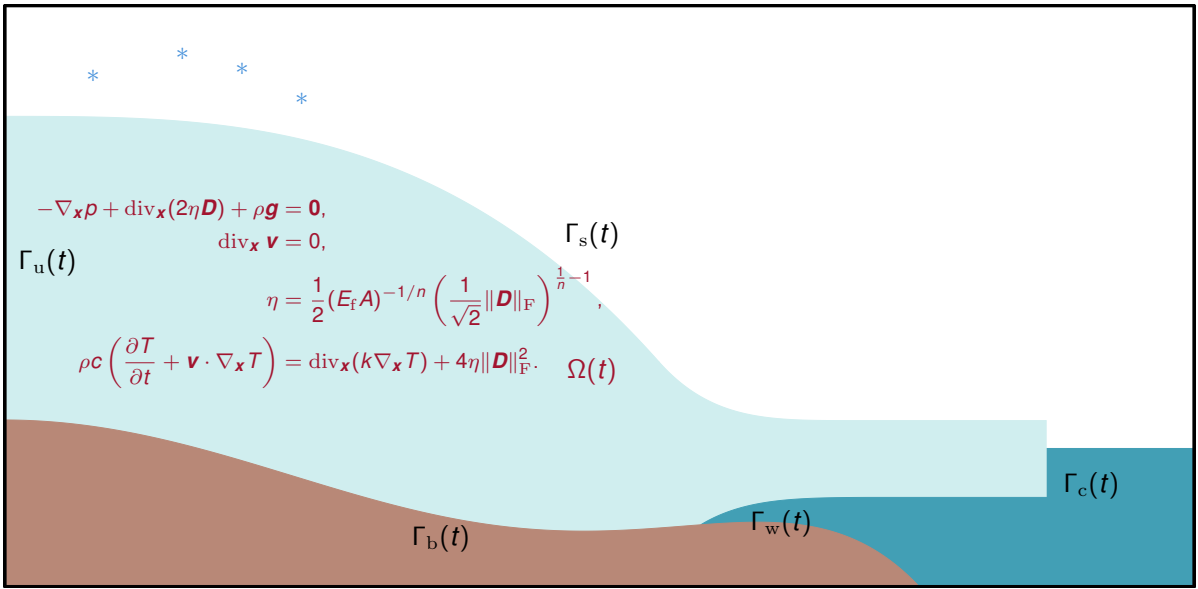

Marine ice-sheet dynamics: Full-order model

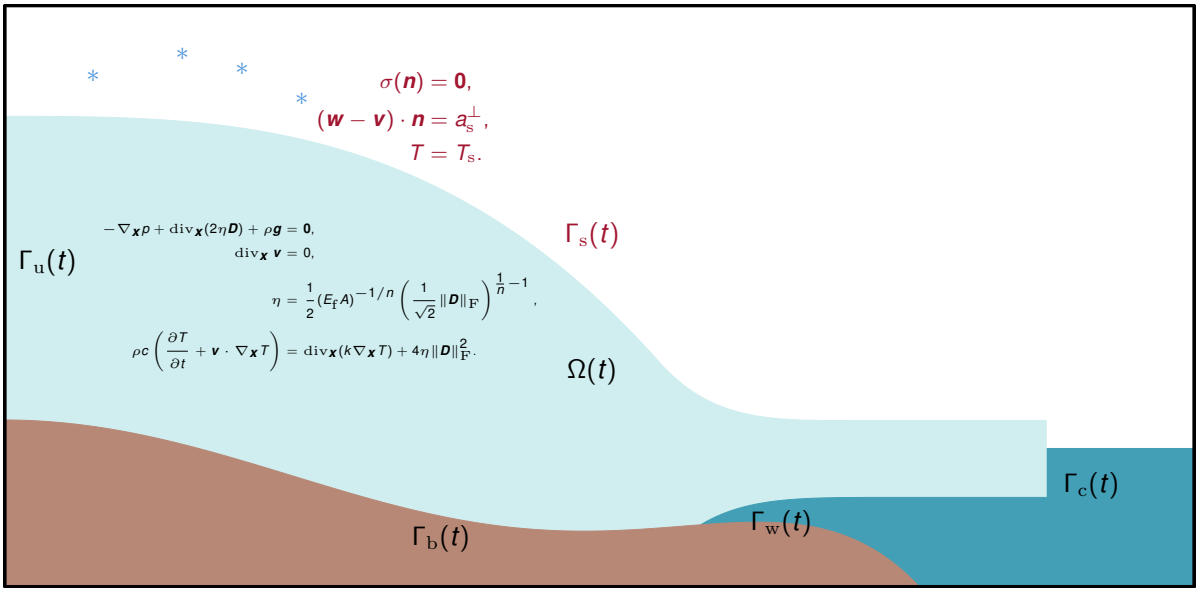

Marine ice-sheet dynamics: Full-order model

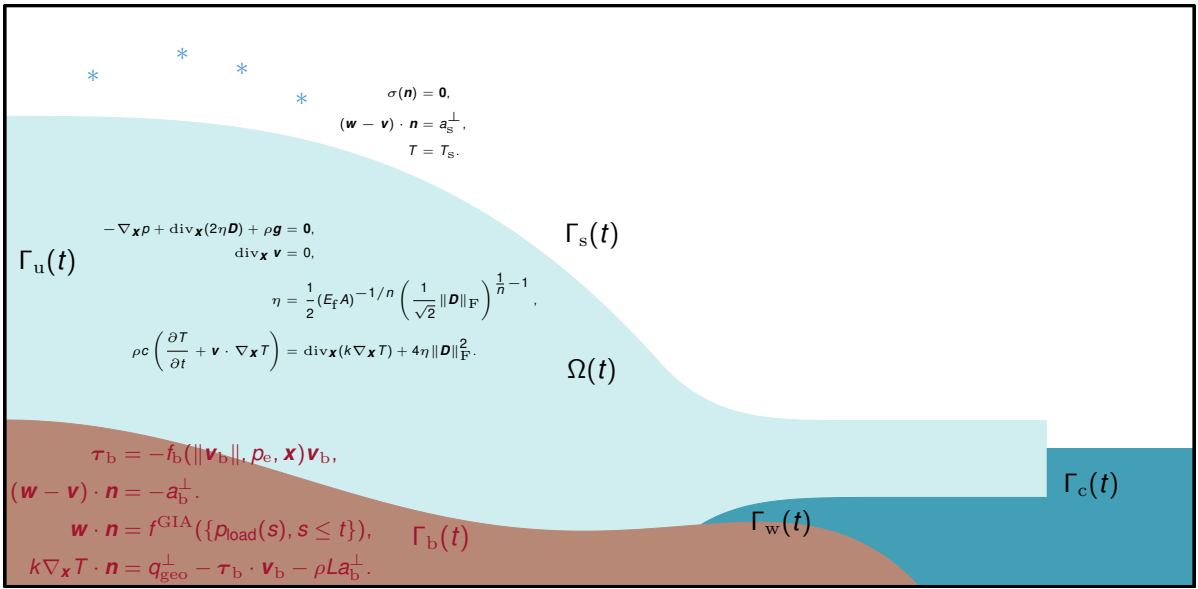

Marine ice-sheet dynamics: Full-order model

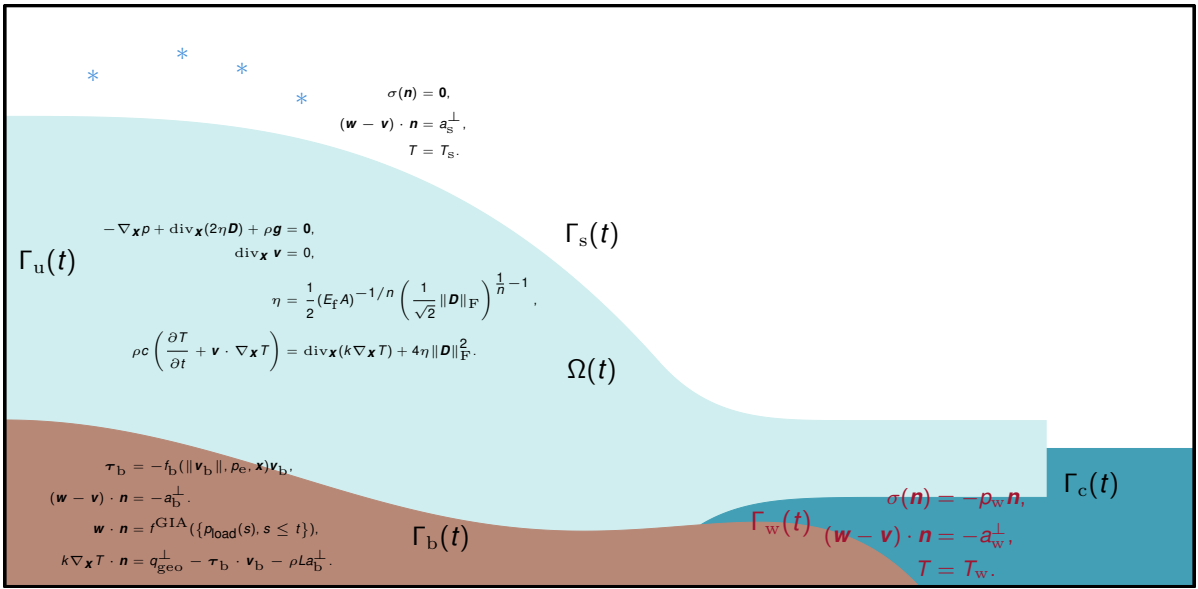

Marine ice-sheet dynamics: Full-order model

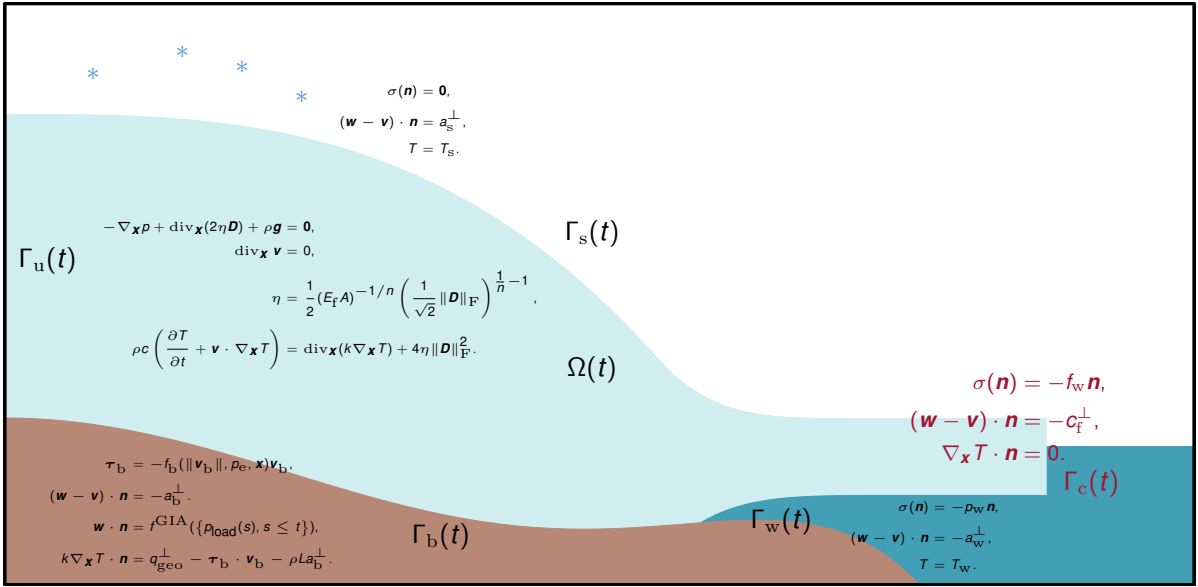

Marine ice sheet instability mechanism

Step 1: Steady state on an upward sloping bed ($q_{\text{in}} = q_{\text{out}}$).

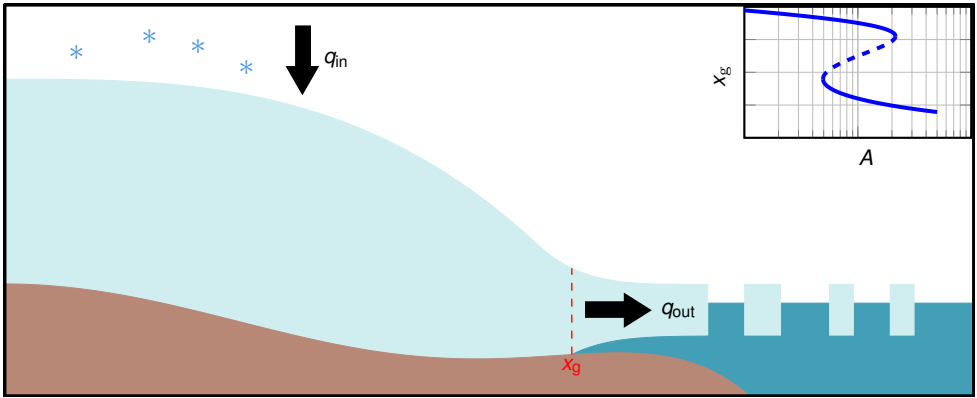

C. Schoof. Ice sheet grounding line dynamics: Steady states, stability and hysteresis. *J. Geophys. Res.*, 2007.
L. Favier. Retreat of Pine Island Glacier controlled by marine ice-sheet instability. *Nat. Clim. Change*, 2014.

Marine ice sheet instability mechanism

Step 2: Initiation of grounding-line retreat ($q_{\text{in}} < q_{\text{out}}$).

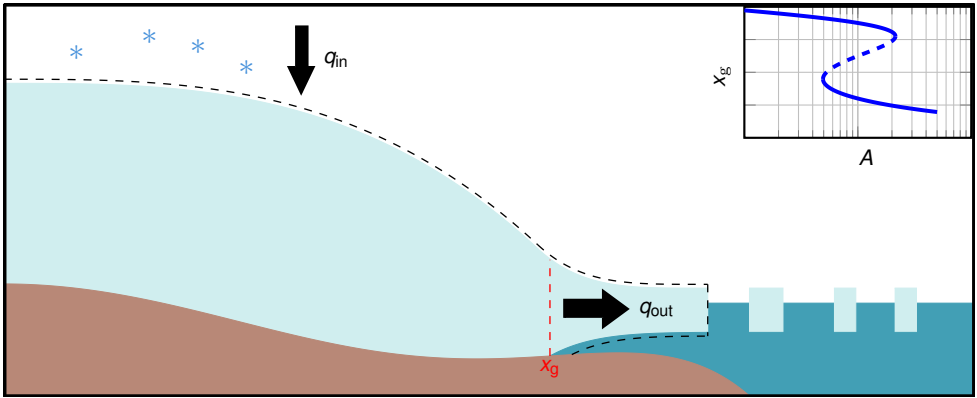

C. Schoof. Ice sheet grounding line dynamics: Steady states, stability and hysteresis. *J. Geophys. Res.*, 2007.
L. Favier. Retreat of Pine Island Glacier controlled by marine ice-sheet instability. *Nat. Clim. Change*, 2014.

Marine ice sheet instability mechanism

Step 3: Self-sustained grounding-line retreat ($q_{\text{in}} \ll q_{\text{out}}$).

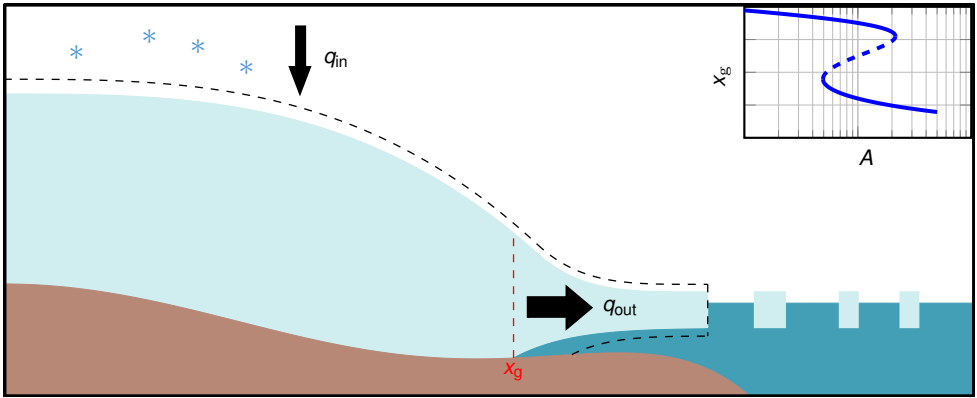

C. Schoof. Ice sheet grounding line dynamics: Steady states, stability and hysteresis. *J. Geophys. Res.*, 2007.
L. Favier. Retreat of Pine Island Glacier controlled by marine ice-sheet instability. *Nat. Clim. Change*, 2014.

Marine ice sheet instability mechanism

Step 4: New steady state on a downward sloping bed ($q_{\text{in}} = q_{\text{out}}$).

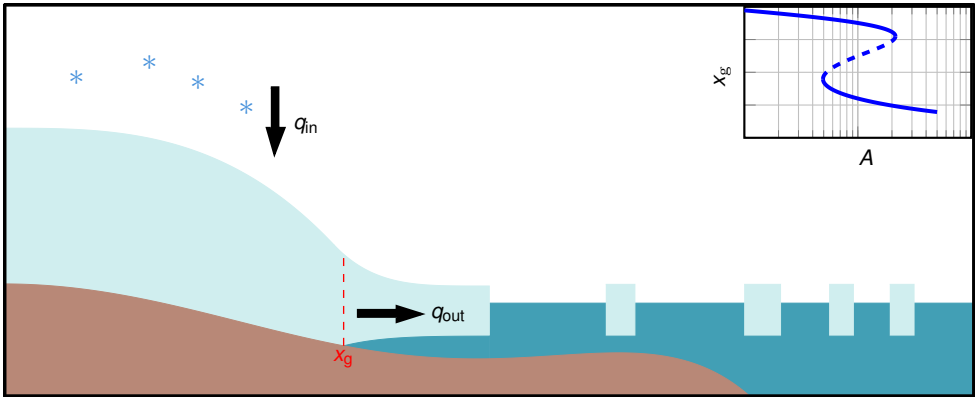

C. Schoof. Ice sheet grounding line dynamics: Steady states, stability and hysteresis. *J. Geophys. Res.*, 2007.
L. Favier. Retreat of Pine Island Glacier controlled by marine ice-sheet instability. *Nat. Clim. Change*, 2014.

Marine ice cliff instability mechanism

Step 1: Hydrofracturing weakens ice shelf.

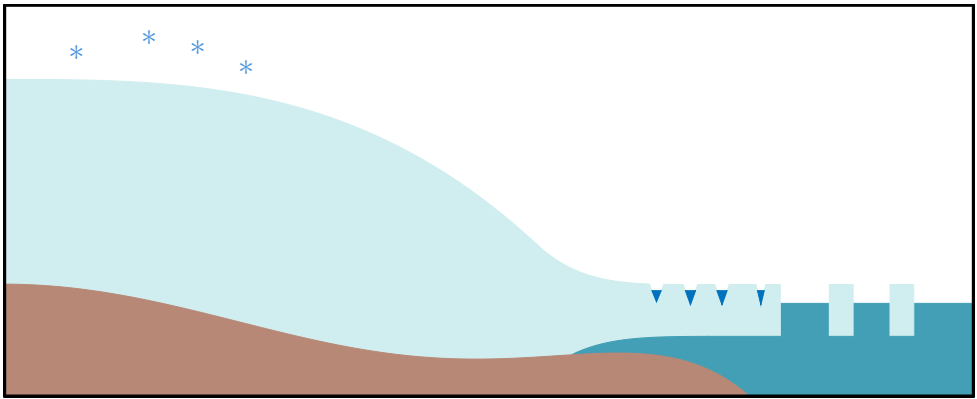

D. Pollard et al. Potential Antarctic Ice Sheet retreat driven by hydrofracturing and ice cliff failure. *Earth Planet. Sc. Lett.*, 2015.

Marine ice cliff instability mechanism

Step 2: Collapse of ice-shelf due to hydrofracturing.

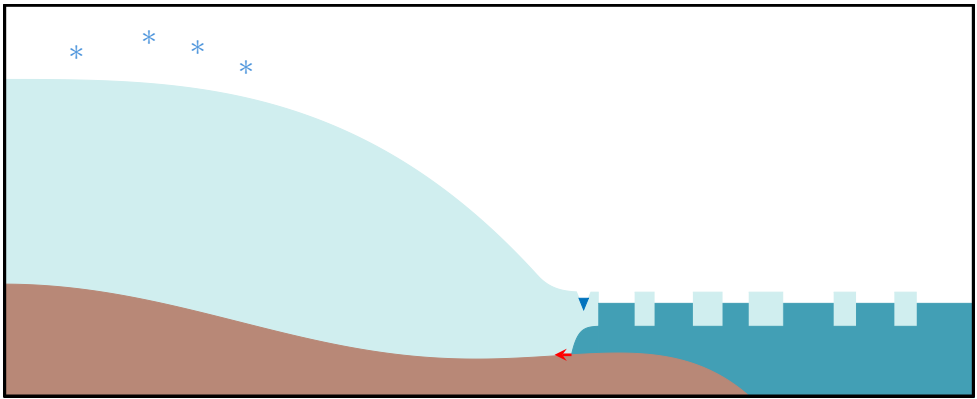

D. Pollard et al. Potential Antarctic Ice Sheet retreat driven by hydrofracturing and ice cliff failure. *Earth Planet. Sc. Lett.*, 2015.

Marine ice cliff instability mechanism

Step 3: Unstable ice cliff (structural failure).

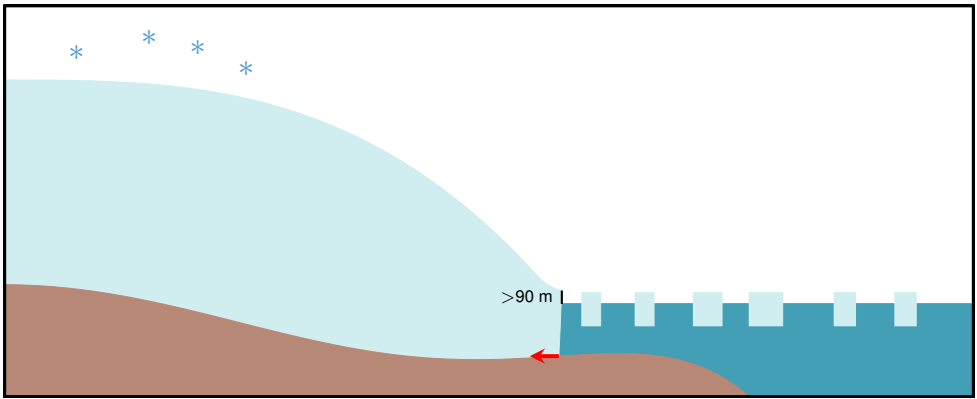

D. Pollard et al. Potential Antarctic Ice Sheet retreat driven by hydrofracturing and ice cliff failure. *Earth Planet. Sc. Lett.*, 2015.

Marine ice cliff instability mechanism

Step 4: Ice-cliff desintegration triggers MICI.

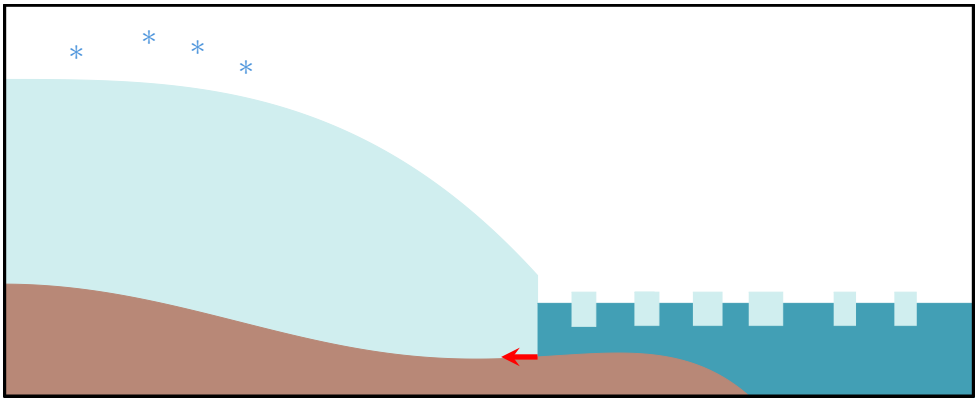

D. Pollard et al. Potential Antarctic Ice Sheet retreat driven by hydrofracturing and ice cliff failure. *Earth Planet. Sc. Lett.*, 2015.

The f.ETISh ice-sheet model

F. Pattyn. Sea-level response to melting of Antarctic ice shelves on multi-centennial timescales with the fast Elementary Thermomechanical Ice Sheet model (f.ETISh v1.0). *Cryosphere*, 11(4), 1851-1878, 10.5194/tc-11-1851-2017.

Fast Elementary Thermomechanical Ice Sheet model (f.ETISh)

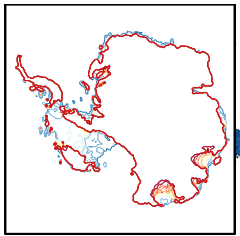

Grounding-line migration + MISI

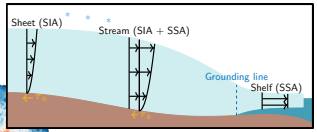

Shallow flow models

$$\frac{\partial T}{\partial t} + \boldsymbol{v} \cdot \nabla_{\boldsymbol{x}} T = \kappa \Delta_{\boldsymbol{x}} T + \frac{4\eta}{\rho c} \dot{d}_{\mathrm{e}}^2$$
$$\eta = \tfrac{1}{2} A(T)^{-1/n} \dot{d}_{\mathrm{e}}^{1/n-1}$$

Thermomechanical coupling

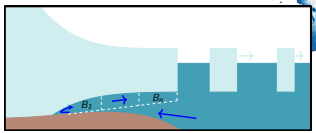

Sub-shelf melting (PICO model) + calving

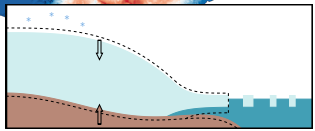

Isostatic bedrock adjustment

- Captures essential characteristics of ice-sheet thermomechanics and ice-stream flow.
- Captures processes controlling grounding-line motion at coarse resolutions via a flux condition.
- Efficient for large-scale and long-term simulations and large-ensemble simulations.

Input data: Present-day geophysical datasets

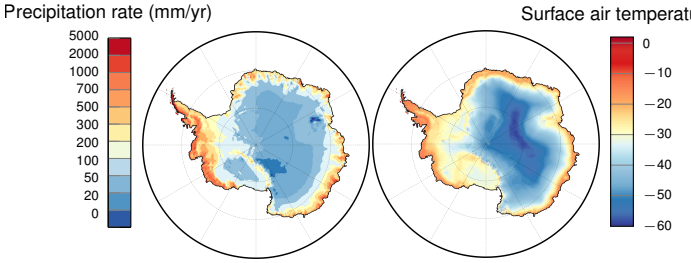

Atmospheric conditions [Van Wessem et al., 2014]

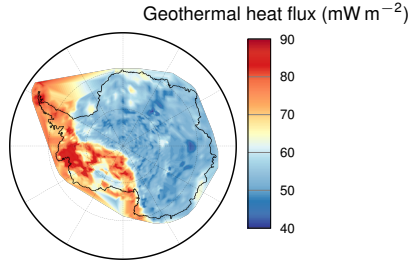

Geothermal heat flux [An et al., 2015]

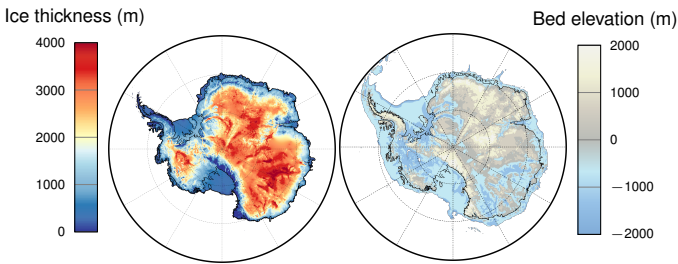

Topography [Fretwell et al., 2013]

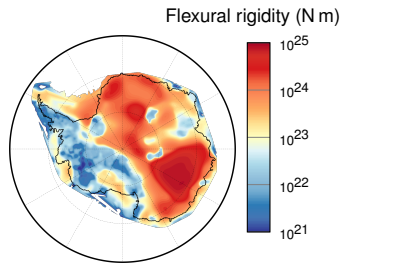

Flexural rigidity [Chen et al., 2018]

Ice-sheet model initialisation: Inversion of basal sliding conditions

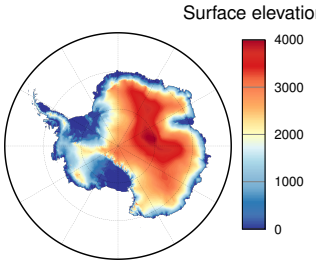

Surface elevation

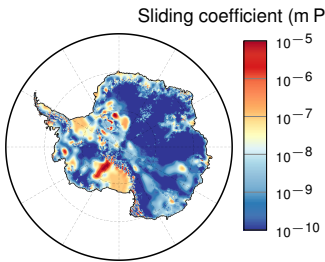

Optimised basal sliding coefficient

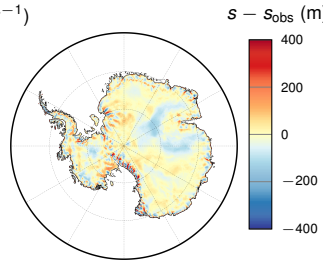

Data misfit

- Power-law friction (Weertman's friction law): $\boldsymbol{\tau}_{\mathrm{b}} = -c_{\mathrm{b}}(\boldsymbol{x}) \| \boldsymbol{v}_{\mathrm{b}} \|^{\frac{1}{m}-1} \boldsymbol{v}_{\mathrm{b}}$.
- The basal sliding coefficient ($A_b = c_b^{-m}$) is obtained by solving an inverse problem that seeks to match the observed present-day ice-sheet surface elevation while assuming that the ice sheet is in steady state (fixed-point iteration scheme):

$$A_{\mathrm{b}}^{(i+1)} = A_{\mathrm{b}}^{(i)} \times 10^{\frac{s^{(i)} - s_{\mathrm{obs}}}{h_{\mathrm{inv}}}}.$$

D. Pollard and R. M. DeConto. A simple inverse method for the distribution of basal sliding coefficients under ice sheets, applied to Antarctica. *Cryosphere*, 2012.

Overview of uncertainty quantification methods

C. Soize. *Uncertainty Quantification: An accelerated Course with Advanced Applications in Computational Engineering*. Springer, 2017.
R. Ghanem et al., Eds. *Handbook of Uncertainty Quantification*. Springer, 2017.
M. Arnst and J.-P. Ponthot. An overview of nonintrusive characterization, propagation, and sensitivity analysis of uncertainties in computational mechanics. *Int. J. Uncertain. Quantif.*, 2014.

Uncertainty quantification: framework

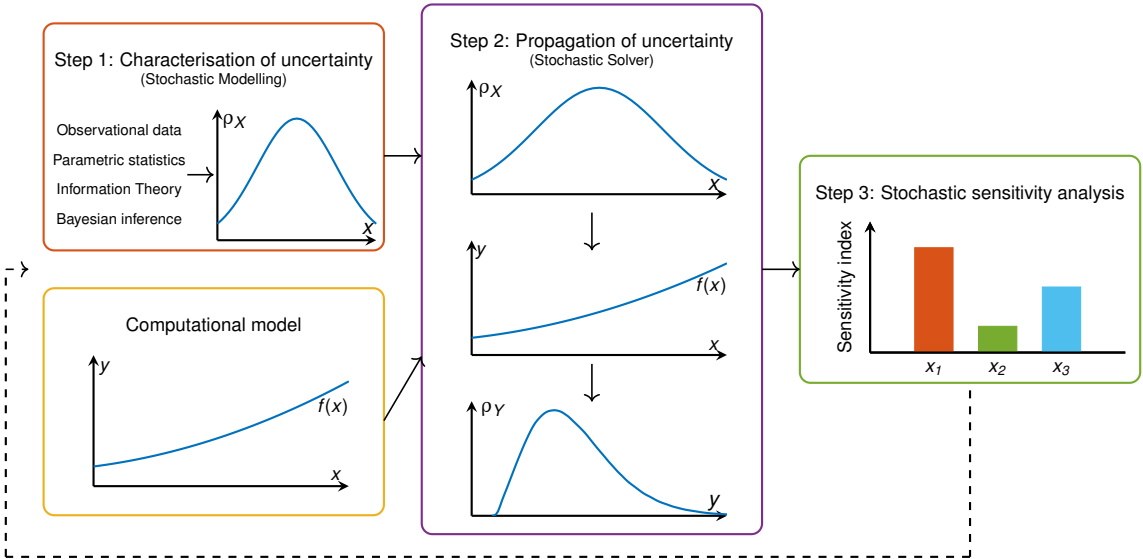

Propagation of uncertainty: Monte Carlo

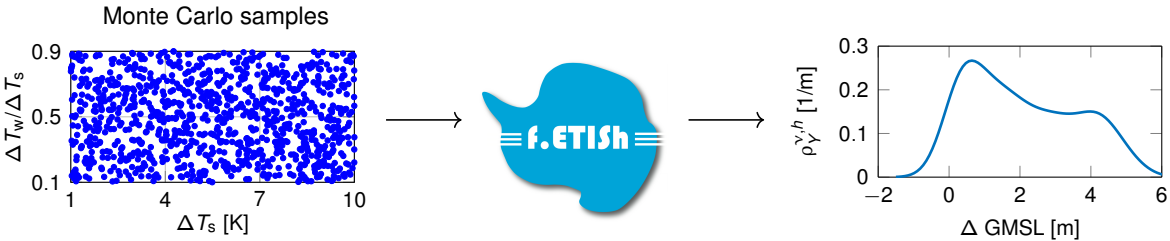

Propagation of uncertainty: Surrogate model

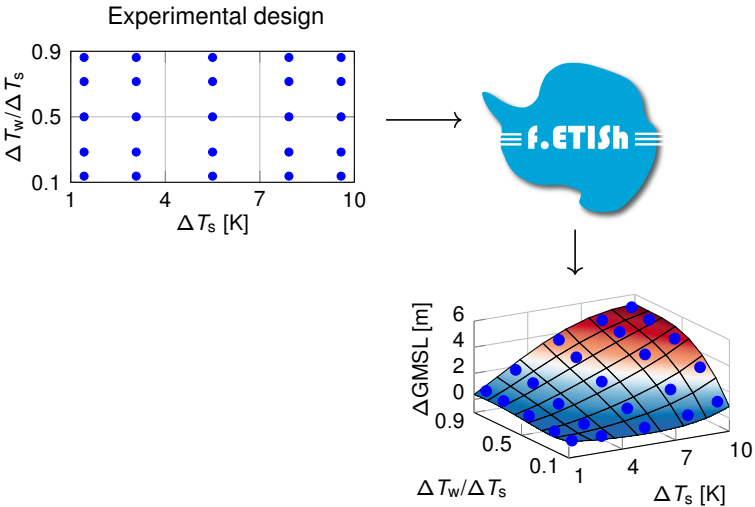

Propagation of uncertainty: Surrogate model

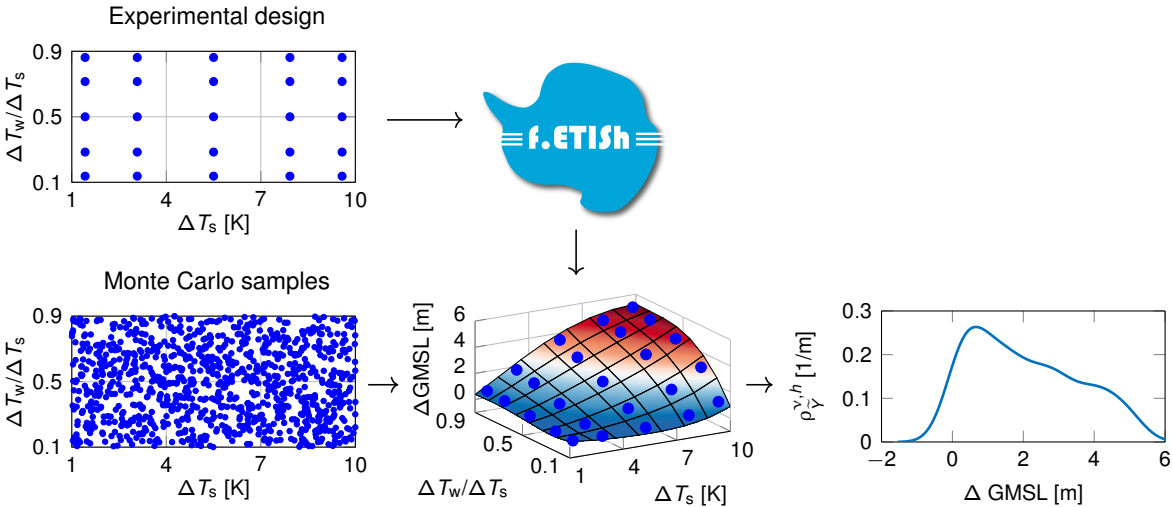

Multifidelity estimation of confidence sets of random excursion sets

K. Bulthuis, F. Pattyn, and M. Arnst. A multifidelity quantile-based approach for confidence sets of random excursion sets with application to ice-sheet dynamics. *SIAM/ASA JUQ*, Under review.

Motivation

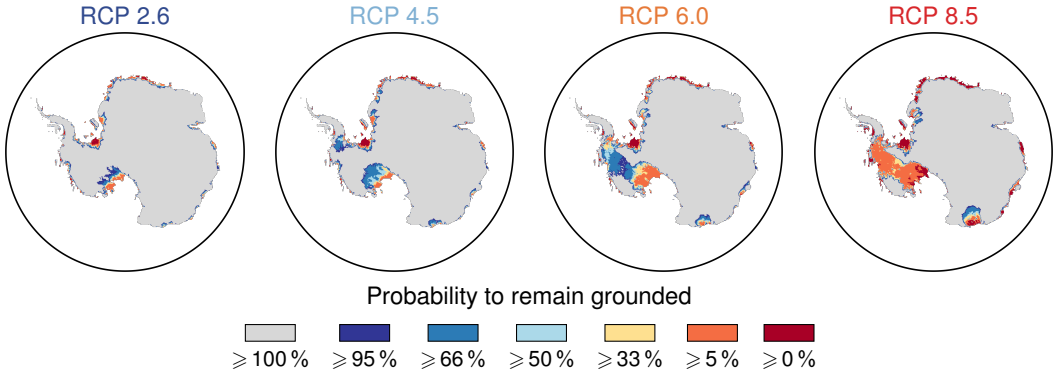

- Motivation: “Risk-assessment” maps to quantify with uncertainty the AIS retreat.
- Framework: Uncertainty quantification of excursion sets with confidence sets.
- Literature: Confidence sets were introduced in the context of Gaussian-process regression + Theory of random sets.
- Challenges: We consider excursion sets of the spatial response of stochastic computational models $\Rightarrow$ New challenges: discretisation of the spatial and stochastic dimensions and high computational cost of the computational model.

Motivation

- In shallow-ice models, the grounded portion of the AIS is the region where the ice thickness is in excess of floatation:

$$D_{\mathrm{g}} = \left\{ \boldsymbol{x} \in D : y(\boldsymbol{x}) = h(\boldsymbol{x}) + \frac{\rho_{\mathrm{w}}}{\rho} b(\boldsymbol{x}) \geq 0 \right\},$$

  that is, the grounded portion is the positive 0-excursion set of the so-called height above floatation $h + \frac{\rho_{\mathrm{w}}}{\rho} b$.

- Question: How to quantify the uncertainty in the grounded portion of the AIS as predicted with computational ice-sheet models?

- Framework: Uncertainty quantification of the spatial response of computational models.

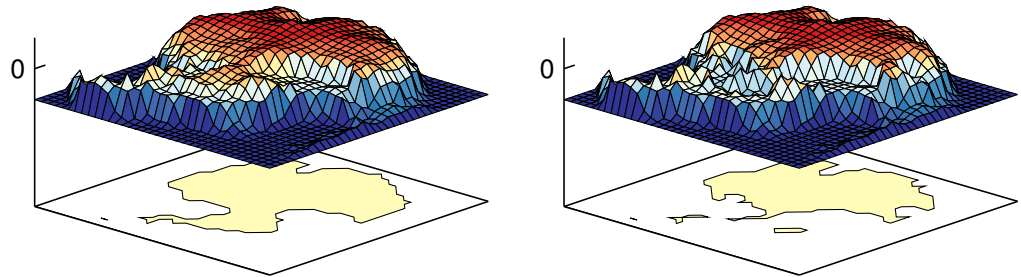

Problem setting

- Let $\{Y(\mathbf{x}), \mathbf{x} \in D\}$ be a random field defined on a probability space $(\Theta, \mathfrak{U}, \mathbb{P})$, indexed by $D \subset \mathbb{R}^d$ ($d \geq 1$), with values in $\mathbb{R}$ and with continuous paths almost surely.
- Positive excursion set:

$$\mathcal{E}_u^+ = \{\mathbf{x} \in D : Y(\mathbf{x}) \geq u\},$$

  where u is a threshold of interest. The set $\mathcal{E}_u^+$ defines a random closed set in $\mathbb{R}^d$.
- Objective: Characterise the variability/uncertainty in the random closed set $\mathcal{E}_u^+$.

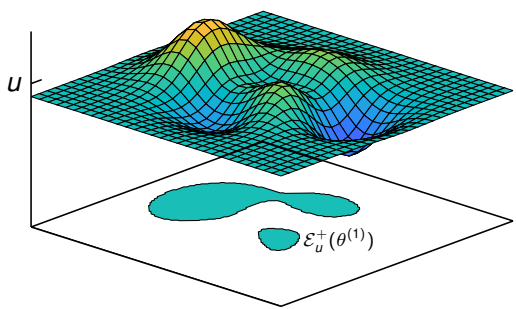

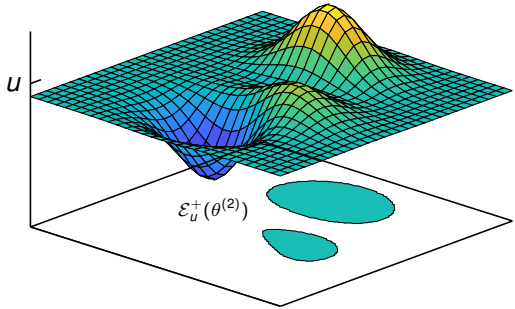

I. Molchanov. *Theory of Random Sets*. Springer, 2017.

Confidence sets

$\mathcal{E}_u^+ \subset C_\alpha^{\text{out}}, C_\alpha^{\text{in}} \subset \mathcal{E}_u^+$

$\mathcal{E}_u^+ \not\subset C_\alpha^{\text{out}}, C_\alpha^{\text{in}} \subset \mathcal{E}_u^+$

$\mathcal{E}_u^+ \subset C_\alpha^{\text{out}}, C_\alpha^{\text{in}} \not\subset \mathcal{E}_u^+$

- Random excursion sets may be characterised by using confidence sets that either contain or are contained within the random excursion set with a given probability level.
- A closed set $C_\alpha^{\text{out}} \in \mathfrak{F}$ is an outer confidence set for $\mathcal{E}_u^+$ with probability at least α if

$$\mathbb{P}\left(\mathcal{E}_u^+ \subset C_\alpha^{\text{out}}\right) \geq \alpha.$$

- An open set $C_\alpha^{\text{in}} \in \mathfrak{L}$ is an inner confidence set for $\mathcal{E}_u^+$ with probability at least α if

$$\mathbb{P}\left(\text{cl}\left(C_\alpha^{\text{in}}\right) \subset \mathcal{E}_u^+\right) \geq \alpha.$$

D. Bolin and F. Lindgren. Excursion and contour uncertainty regions for latent Gaussian models. *J. Royal Stat. Soc. B*, 2015.
I. Molchanov. *Theory of Random Sets*. Springer, 2017.

Parametric family of candidate sets

- Confidence sets are sought in a parametric family of candidate sets $\{T_\rho, \rho \in (0,1)\}$ taken as the superlevel sets of a so-called membership function $T : D \to [0,1]$, that is,

$$T_\rho = \{\mathbf{x} \in \mathrm{int}(D) : T(\mathbf{x}) > \rho\}, \quad \text{for } \rho \in (0,1).$$

- The confidence set is identified in this parametric family of candidate sets such that

$$\rho^* = \arg\min_{T_\rho} |T_\rho| \text{ subject to } \mathbb{P}\left(\mathrm{cl}\left(T_\rho\right) \subset \mathcal{E}_u^+\right) \geq \alpha.$$

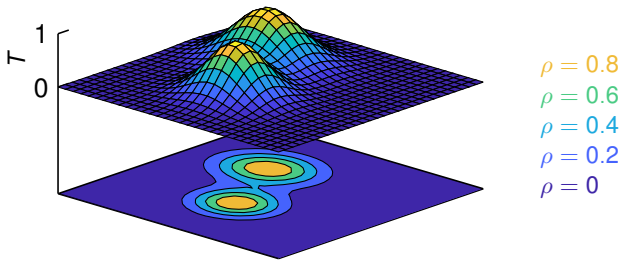

D. Bolin and F. Lindgren. Excursion and contour uncertainty regions for latent Gaussian models. *J. Royal Stat. Soc. B*, 2015.

Evaluation of a confidence set in a parametric family of sets

1) Determine a membership function T for the random field:
   - T should (1) quantify the difference between the random field and the threshold u and (2) account for the uncertainty in the random field.
   - Examples for T based on first-order statistical descriptors of the random field:

$$T_1(\mathbf{x}) = \mathbb{P}(Y(\mathbf{x}) \geq u),\ T_2(\mathbf{x}) = \frac{1}{2}\left(1 + \operatorname{erf}\left(\frac{\mathbb{E}[Y(\mathbf{x})] - u}{\sqrt{2\mathbb{V}[Y(\mathbf{x})]}}\right)\right),\ T_3(\mathbf{x}) = \frac{1}{2}\left(1 + \frac{\mathbb{E}[Y(\mathbf{x})] - u}{\sqrt{\mathbb{E}[(Y(\mathbf{x}) - u)^2]}}\right).$$

2) Solve an optimisation problem:
   - The optimal threshold ρ^* satisfies

$$\rho^* = \inf_{\rho \in (0,1)} \rho \text{ subject to } \mathbb{P}\left(\mathrm{cl}\left(T_\rho\right) \subset \mathcal{E}_u^+\right) \geq \alpha.$$

   - The evaluation of the inclusion probability can be computationally expensive unless the problem is restricted to simple random fields.

D. Bolin and F. Lindgren. Excursion and contour uncertainty regions for latent Gaussian models. *J. Royal Stat. Soc. B*, 2015.
J. P. French and J. A. Hoeting. Credible regions for exceedance sets of geostatistical data. *Environmetrics*, 2015.

Equivalent problem of quantile estimation

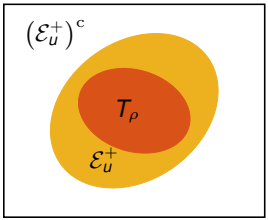

$$\mathbb{P}(T_\rho \subset \mathcal{E}_u^+) \geq \alpha$$
$$\mathbb{P}\left((\mathcal{E}_u^+)^c \subset T_\rho^c\right) \geq \alpha$$
$$\mathbb{P}\left(T(\boldsymbol{x}) \leq \rho, \boldsymbol{x} \in (\mathcal{E}_u^+)^c\right) \geq \alpha$$
$$\mathbb{P}\left(\sup_{\boldsymbol{x} \in (\mathcal{E}_u^+)^c} T(\boldsymbol{x}) \leq \rho\right) \geq \alpha$$

- The identification of the largest confidence set in a parametric family of candidate sets is recast as a quantile estimation problem of a random variable taken as the supremum of the membership function over the complement of the random excursion set:

$$\rho^* = \inf\{\rho \in (0,1) : F_\chi(\rho) \geq \alpha\} \equiv q_\chi(\alpha),$$

with

$$\chi = \sup_{\boldsymbol{x} \in (\mathcal{E}_u^+)^c} T(\boldsymbol{x}).$$

J. P. French and J. A. Hoeting. Credible regions for exceedance sets of geostatistical data. *Environmetrics*, 2015.

Spatial discretisation

- Let $D^h = \left\{D_i^h\right\}_{1 \le i \le N_h}$ be a partition of D and for each i, let $\boldsymbol{x}_i^h$ be a representative point in D_i^h.
- Discretisation as simple random closed set:

$$\mathcal{E}_u^{+h} = \bigcup_{E_i^h = 1} D_i^h = \bigcup_{i \in \mathcal{I}_u^{+h}} D_i^h \quad \left(\mathcal{I}_u^{+h} = \left\{i : E_i^h = \mathbf{1}(Y(\boldsymbol{x}_i^h) \ge u) = 1\right\}\right).$$

- Discretisation of the parametric family of candidate sets:

$$\mathrm{cl}\left(T_\rho^h\right) = \bigcup_{T_{\rho,i}^h = 1} D_i^h = \bigcup_{i \in I_\rho^h} D_i^h \quad \left(I_\rho^h = \left\{i : T_{\rho,i}^h = \mathbf{1}(T(\boldsymbol{x}_i^h) > \rho) = 1\right\}\right).$$

- Quantile estimation problem of a discrete random variable:

$$\rho^* = \inf\left\{\rho \in (0,1) : F_{\chi^h}(\rho) \ge \alpha\right\} \equiv q_{\chi^h}(\alpha),$$

with $\chi^h = \max_{i \in \left(\mathcal{I}_u^{+h}\right)^c} T_i^h$.

$\mathcal{E}_u^+$

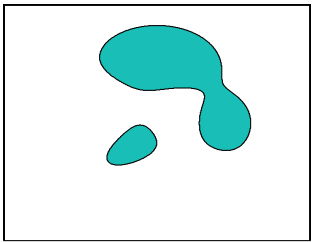

$\mathcal{E}_u^{+h}$

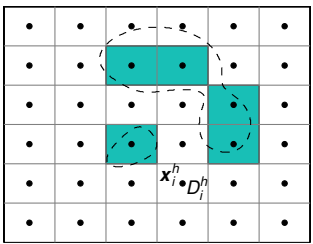

Evaluation of confidence sets: Computational aspects

- Let $\{Y(\mathbf{x}), \mathbf{x} \in D\}$ be the response of a stochastic computational model that depends on an $\mathbb{R}^n$-valued random vector $\boldsymbol{\xi} = (\xi_1, \ldots, \xi_n)$.
- Evaluation of a first-order statistical descriptor T of the random field:
  - For each $\mathbf{x} \in D$, build an approximation of $T(\mathbf{x})$ using standard nonintrusive methods for uncertainty quantification (Monte Carlo sampling, spectral expansions, kriging, ...).
- Estimation of the α-quantile of the random variable χ:
  - Link with the computation of failure probability in reliability engineering:

$$F_\chi(\rho) = \mathbb{P}(\chi \leq \rho) = \int_{\Theta_\rho} d\mathbb{P}(\theta) = \int_\Theta \mathbf{1}(\theta \in \Theta_\rho) d\mathbb{P}(\theta),$$

    where the event

$$\Theta_\rho = \{\theta \in \Theta : \chi(\theta) - \rho \leq 0\}$$

    is defined by the limit state function $\chi - \rho$.
  - Methods from reliability engineering to compute failure probability include Monte Carlo estimation, surrogate-based methods, and multifidelity methods.

Quantile estimation: Monte Carlo method

- Monte Carlo estimation:

$$q_\chi^\nu(\alpha) = \inf\left\{\rho \in (0,1) : F_\chi^\nu(\rho) \geq \alpha\right\}, \text{where } F_\chi^\nu(\rho) = \frac{1}{\nu}\sum_{k=1}^{\nu} \mathbf{1}\left(\chi(\theta^{(k)}) \leq \rho\right)$$

  is the sample distribution function built on the i.i.d. samples $\left\{\chi(\theta^{(k)}), 1 \leq k \leq \nu\right\}$ of χ.

- When χ is a discrete random variable, use the mid-distribution function.
- Computational cost: The approximation error is $\mathcal{O}(\sqrt{\alpha(1-\alpha)}/\sqrt{\nu})$.

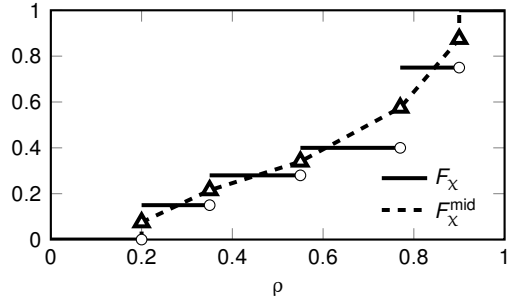

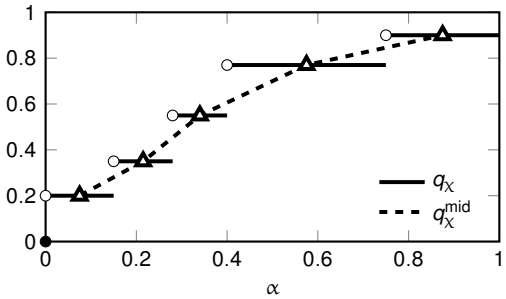

Ma et al. Asymptotic properties of sample quantiles of discrete distributions. *Ann. I. Stat. Math.*, 2011.

Quantile estimation: Spectral method

a) Indirect approach: Spectral representation of the random field:

1) Polynomial chaos expansion of order p of the random field:

$$Y^p(\mathbf{x}) = \sum_{|\boldsymbol{\alpha}|=0}^{p} y_{\boldsymbol{\alpha}}^p(\mathbf{x})\, \psi_{\boldsymbol{\alpha}}(\boldsymbol{\xi}).$$

2) Approximation of the random excursion set:

$$\mathcal{E}_u^{+,p} = \left\{\mathbf{x} \in D : Y^p(\mathbf{x}) \geq 0\right\}.$$

3) Approximation of the random variable χ:

$$\sup_{\mathbf{x} \in \left(\mathcal{E}_u^{+,p}\right)^c} T(\mathbf{x}).$$

b) Direct approach: Spectral representation of the random variable χ:

$$\chi^p = \sum_{|\boldsymbol{\alpha}|=0}^{p} \chi_{\boldsymbol{\alpha}}^p\, \psi_{\boldsymbol{\alpha}}(\boldsymbol{\xi}).$$

- This approach is enabled by the reformulation of the optimisation problem for confidence sets as a problem of quantile estimation of a random variable.

Surrogate-based quantile estimation: Approximation error

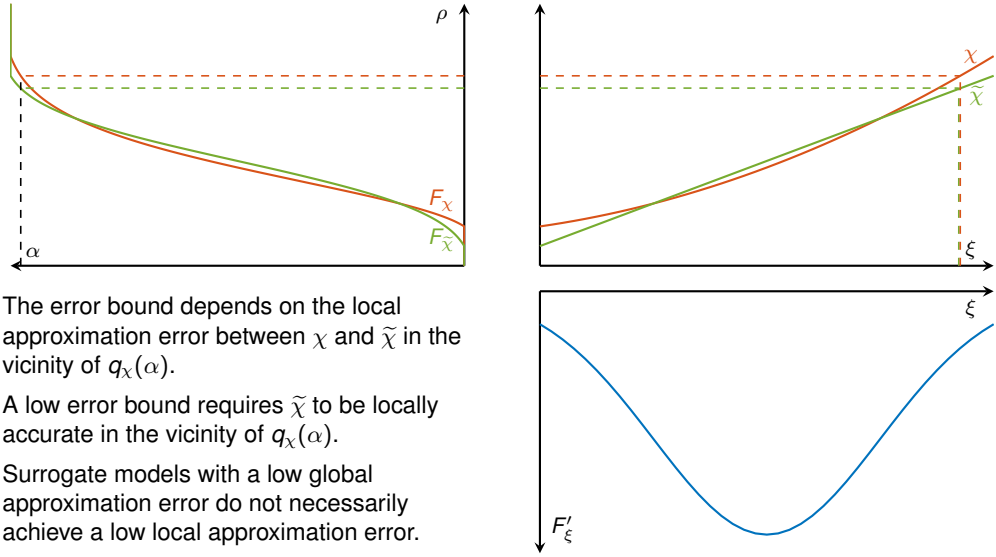

- The error bound depends on the local approximation error between χ and $\widetilde{\chi}$ in the vicinity of $q_\chi(\alpha)$.
- A low error bound requires $\widetilde{\chi}$ to be locally accurate in the vicinity of $q_\chi(\alpha)$.
- Surrogate models with a low global approximation error do not necessarily achieve a low local approximation error.

G. C. Enss et al. Nonparametric quantile estimation based on surrogate models. *IEEE T. Inform. Theory*, 2016.

Quantile estimation: bifidelity approach

- To reduce the required number of evaluations of the computational model and the approximation error, the quantile estimation problem is solved by using a computationally efficient bifidelity method that exploits the bifidelity model

$$\widetilde{\chi}^{\gamma} = \underbrace{\widetilde{\chi}\,\mathbf{1}\left(|\widetilde{\chi} - q_{\chi}(\alpha)| > \gamma\right)}_{\text{Surrogate model used further away from the quantile}} + \underbrace{\chi\,\mathbf{1}\left(|\widetilde{\chi} - q_{\chi}(\alpha)| \leq \gamma\right)}_{\text{Surrogate model used closer to the quantile}} .$$

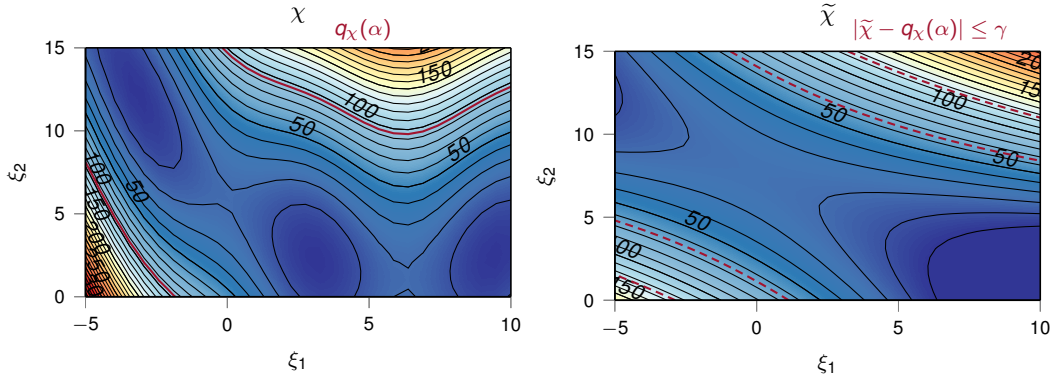

J. Li and D. Xiu. Evaluation of failure probability via surrogate models. *J. Comput. Phys.*, 2010.

Bifidelity approach: Iterative algorithm

Algorithm Iterative algorithm for the bifidelity method

Initialisation:

1. Build a surrogate model $\widetilde{\chi}$ of χ.
2. Draw ν i.i.d. samples to obtain $S = \left\{\boldsymbol{\xi}(\theta^{(k)}), 1 \leq k \leq \nu\right\}$.
3. Set $k = 0$, $\widetilde{S}^{(0)} = S$, $\Delta\nu \ll \nu$ (step size), and $\eta \geq 0$.
4. Evaluate $\left\{\widetilde{\chi}(\theta^{(k)}), 1 \leq k \leq \nu\right\}$.
5. Set $q^{(0)}(\alpha)$ as the α-quantile of $\left\{\widetilde{\chi}(\theta^{(k)}), 1 \leq k \leq \nu\right\}$.

Iteration: at the j-th iteration ($j \geq 1$), **do**:

1. Sort $\left\{|\widetilde{\chi}(\theta^{(k)}) - q^{(j-1)}(\alpha)|, \theta^{(k)} \in \widetilde{S}^{(j-1)}\right\}$ in ascending order. Let $\Delta\widetilde{S}^{(j)}$ be the $\Delta\nu$ smallest elements and $\widetilde{S}^{(j)} = \widetilde{S}^{(j-1)} \backslash \Delta\widetilde{S}^{(j)}$.
2. Evaluate $\chi(\theta^{(k)})$ and set $\widetilde{\chi}(\theta^{(k)}) = \chi(\theta^{(k)}), \forall \theta^{(k)} \in \Delta\widetilde{S}^{(j)}$.
3. Set $q^{(j)}(\alpha)$ as the α-quantile of $\left\{\widetilde{\chi}(\theta^{(k)}), 1 \leq k \leq \nu\right\}$.
4. If $|q^{(j)}(\alpha) - q^{(j-1)}(\alpha)| \leq \eta$ or $\widetilde{S}^{(j)} = \emptyset$, exit; otherwise increment j by 1.

Return $q^{(j)}(\alpha)$ as an estimate of $q_\chi(\alpha)$.

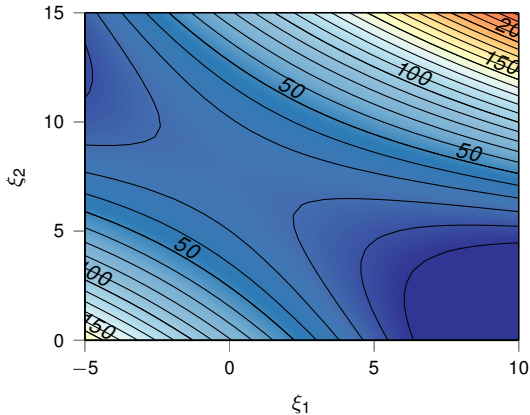

Bifidelity approach: Iterative algorithm

Algorithm Iterative algorithm for the bifidelity method

Initialisation:

1. Build a surrogate model $\widetilde{\chi}$ of χ.
2. Draw ν i.i.d. samples to obtain $S = \left\{\boldsymbol{\xi}(\theta^{(k)}), 1 \leq k \leq \nu\right\}$.
3. Set $k = 0$, $\widetilde{S}^{(0)} = S$, $\Delta\nu \ll \nu$ (step size), and $\eta \geq 0$.
4. Evaluate $\left\{\widetilde{\chi}(\theta^{(k)}), 1 \leq k \leq \nu\right\}$.
5. Set $q^{(0)}(\alpha)$ as the α-quantile of $\left\{\widetilde{\chi}(\theta^{(k)}), 1 \leq k \leq \nu\right\}$.

Iteration: at the j-th iteration ($j \geq 1$), **do**:

1. Sort $\left\{|\widetilde{\chi}(\theta^{(k)}) - q^{(j-1)}(\alpha)|, \theta^{(k)} \in \widetilde{S}^{(j-1)}\right\}$ in ascending order. Let $\Delta\widetilde{S}^{(j)}$ be the $\Delta\nu$ smallest elements and $\widetilde{S}^{(j)} = \widetilde{S}^{(j-1)} \backslash \Delta\widetilde{S}^{(j)}$.
2. Evaluate $\chi(\theta^{(k)})$ and set $\widetilde{\chi}(\theta^{(k)}) = \chi(\theta^{(k)}), \forall \theta^{(k)} \in \Delta\widetilde{S}^{(j)}$.
3. Set $q^{(j)}(\alpha)$ as the α-quantile of $\left\{\widetilde{\chi}(\theta^{(k)}), 1 \leq k \leq \nu\right\}$.
4. If $|q^{(j)}(\alpha) - q^{(j-1)}(\alpha)| \leq \eta$ or $\widetilde{S}^{(j)} = \emptyset$, exit; otherwise increment j by 1.

Return $q^{(j)}(\alpha)$ as an estimate of $q_\chi(\alpha)$.

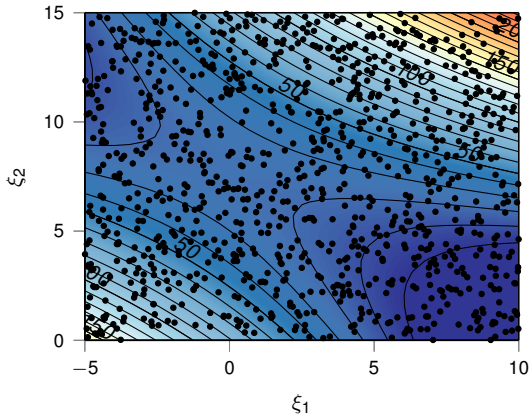

Bifidelity approach: Iterative algorithm

Algorithm Iterative algorithm for the bifidelity method

Initialisation:

1. Build a surrogate model $\widetilde{\chi}$ of χ.
2. Draw ν i.i.d. samples to obtain $S = \left\{\boldsymbol{\xi}(\theta^{(k)}), 1 \leq k \leq \nu\right\}$.
3. Set $k = 0$, $\widetilde{S}^{(0)} = S$, $\Delta\nu \ll \nu$ (step size), and $\eta \geq 0$.
4. Evaluate $\left\{\widetilde{\chi}(\theta^{(k)}), 1 \leq k \leq \nu\right\}$.
5. Set $q^{(0)}(\alpha)$ as the α-quantile of $\left\{\widetilde{\chi}(\theta^{(k)}), 1 \leq k \leq \nu\right\}$.

Iteration: at the j-th iteration ($j \geq 1$), **do**:

1. Sort $\left\{|\widetilde{\chi}(\theta^{(k)}) - q^{(j-1)}(\alpha)|, \theta^{(k)} \in \widetilde{S}^{(j-1)}\right\}$ in ascending order. Let $\Delta\widetilde{S}^{(j)}$ be the $\Delta\nu$ smallest elements and $\widetilde{S}^{(j)} = \widetilde{S}^{(j-1)} \backslash \Delta\widetilde{S}^{(j)}$.
2. Evaluate $\chi(\theta^{(k)})$ and set $\widetilde{\chi}(\theta^{(k)}) = \chi(\theta^{(k)}), \forall \theta^{(k)} \in \Delta\widetilde{S}^{(j)}$.
3. Set $q^{(j)}(\alpha)$ as the α-quantile of $\left\{\widetilde{\chi}(\theta^{(k)}), 1 \leq k \leq \nu\right\}$.
4. If $|q^{(j)}(\alpha) - q^{(j-1)}(\alpha)| \leq \eta$ or $\widetilde{S}^{(j)} = \emptyset$, exit; otherwise increment j by 1.

Return $q^{(j)}(\alpha)$ as an estimate of $q_\chi(\alpha)$.

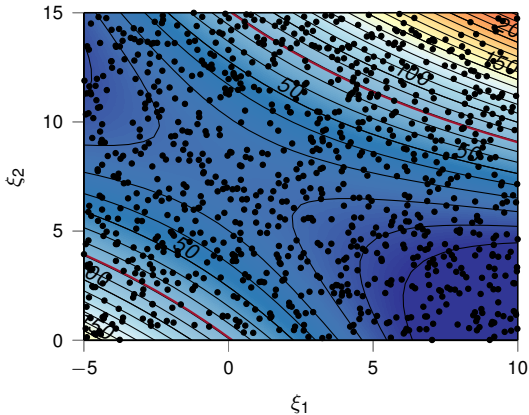

Bifidelity approach: Iterative algorithm

Algorithm Iterative algorithm for the bifidelity method

Initialisation:

1. Build a surrogate model $\widetilde{\chi}$ of χ.
2. Draw ν i.i.d. samples to obtain $S = \left\{\boldsymbol{\xi}(\theta^{(k)}), 1 \leq k \leq \nu\right\}$.
3. Set $k = 0$, $\widetilde{S}^{(0)} = S$, $\Delta\nu \ll \nu$ (step size), and $\eta \geq 0$.
4. Evaluate $\left\{\widetilde{\chi}(\theta^{(k)}), 1 \leq k \leq \nu\right\}$.
5. Set $q^{(0)}(\alpha)$ as the α-quantile of $\left\{\widetilde{\chi}(\theta^{(k)}), 1 \leq k \leq \nu\right\}$.

Iteration: at the j-th iteration ($j \geq 1$), **do**:

1. Sort $\left\{|\widetilde{\chi}(\theta^{(k)}) - q^{(j-1)}(\alpha)|, \theta^{(k)} \in \widetilde{S}^{(j-1)}\right\}$ in ascending order. Let $\Delta\widetilde{S}^{(j)}$ be the $\Delta\nu$ smallest elements and $\widetilde{S}^{(j)} = \widetilde{S}^{(j-1)} \backslash \Delta\widetilde{S}^{(j)}$.
2. Evaluate $\chi(\theta^{(k)})$ and set $\widetilde{\chi}(\theta^{(k)}) = \chi(\theta^{(k)}), \forall \theta^{(k)} \in \Delta\widetilde{S}^{(j)}$.
3. Set $q^{(j)}(\alpha)$ as the α-quantile of $\left\{\widetilde{\chi}(\theta^{(k)}), 1 \leq k \leq \nu\right\}$.
4. If $|q^{(j)}(\alpha) - q^{(j-1)}(\alpha)| \leq \eta$ or $\widetilde{S}^{(j)} = \emptyset$, exit; otherwise increment j by 1.

Return $q^{(j)}(\alpha)$ as an estimate of $q_\chi(\alpha)$.

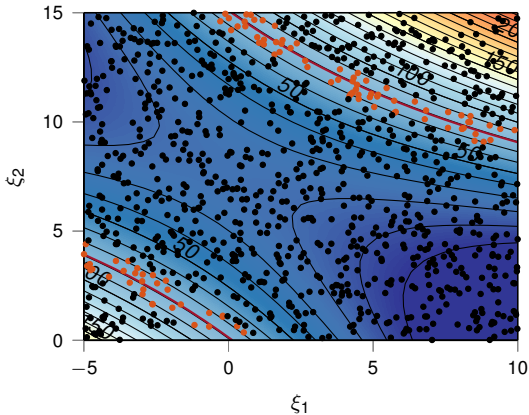

Bifidelity approach: Iterative algorithm

Algorithm Iterative algorithm for the bifidelity method

Initialisation:

1. Build a surrogate model $\widetilde{\chi}$ of χ.
2. Draw ν i.i.d. samples to obtain $S = \left\{\boldsymbol{\xi}(\theta^{(k)}), 1 \leq k \leq \nu\right\}$.
3. Set $k = 0$, $\widetilde{S}^{(0)} = S$, $\Delta\nu \ll \nu$ (step size), and $\eta \geq 0$.
4. Evaluate $\left\{\widetilde{\chi}(\theta^{(k)}), 1 \leq k \leq \nu\right\}$.
5. Set $q^{(0)}(\alpha)$ as the α-quantile of $\left\{\widetilde{\chi}(\theta^{(k)}), 1 \leq k \leq \nu\right\}$.

Iteration: at the j-th iteration ($j \geq 1$), **do**:

1. Sort $\left\{|\widetilde{\chi}(\theta^{(k)}) - q^{(j-1)}(\alpha)|, \theta^{(k)} \in \widetilde{S}^{(j-1)}\right\}$ in ascending order. Let $\Delta\widetilde{S}^{(j)}$ be the $\Delta\nu$ smallest elements and $\widetilde{S}^{(j)} = \widetilde{S}^{(j-1)} \backslash \Delta\widetilde{S}^{(j)}$.
2. Evaluate $\chi(\theta^{(k)})$ and set $\widetilde{\chi}(\theta^{(k)}) = \chi(\theta^{(k)}), \forall \theta^{(k)} \in \Delta\widetilde{S}^{(j)}$.
3. Set $q^{(j)}(\alpha)$ as the α-quantile of $\left\{\widetilde{\chi}(\theta^{(k)}), 1 \leq k \leq \nu\right\}$.
4. If $|q^{(j)}(\alpha) - q^{(j-1)}(\alpha)| \leq \eta$ or $\widetilde{S}^{(j)} = \emptyset$, exit; otherwise increment j by 1.

Return $q^{(j)}(\alpha)$ as an estimate of $q_\chi(\alpha)$.

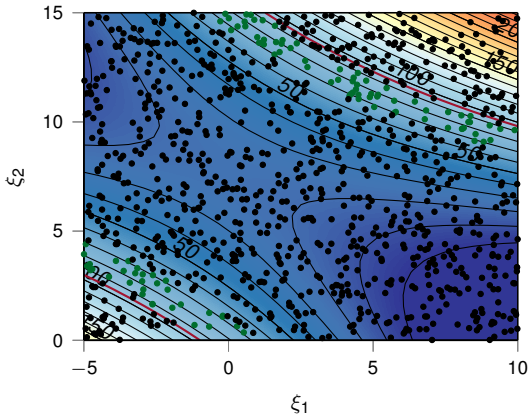

Bifidelity approach: Iterative algorithm

Algorithm Iterative algorithm for the bifidelity method

Initialisation:

1. Build a surrogate model $\widetilde{\chi}$ of χ.
2. Draw ν i.i.d. samples to obtain $S = \left\{\boldsymbol{\xi}(\theta^{(k)}), 1 \leq k \leq \nu\right\}$.
3. Set $k = 0$, $\widetilde{S}^{(0)} = S$, $\Delta\nu \ll \nu$ (step size), and $\eta \geq 0$.
4. Evaluate $\left\{\widetilde{\chi}(\theta^{(k)}), 1 \leq k \leq \nu\right\}$.
5. Set $q^{(0)}(\alpha)$ as the α-quantile of $\left\{\widetilde{\chi}(\theta^{(k)}), 1 \leq k \leq \nu\right\}$.

Iteration: at the j-th iteration ($j \geq 1$), **do**:

1. Sort $\left\{|\widetilde{\chi}(\theta^{(k)}) - q^{(j-1)}(\alpha)|, \theta^{(k)} \in \widetilde{S}^{(j-1)}\right\}$ in ascending order. Let $\Delta\widetilde{S}^{(j)}$ be the $\Delta\nu$ smallest elements and $\widetilde{S}^{(j)} = \widetilde{S}^{(j-1)} \backslash \Delta\widetilde{S}^{(j)}$.
2. Evaluate $\chi(\theta^{(k)})$ and set $\widetilde{\chi}(\theta^{(k)}) = \chi(\theta^{(k)}), \forall \theta^{(k)} \in \Delta\widetilde{S}^{(j)}$.
3. Set $q^{(j)}(\alpha)$ as the α-quantile of $\left\{\widetilde{\chi}(\theta^{(k)}), 1 \leq k \leq \nu\right\}$.
4. If $|q^{(j)}(\alpha) - q^{(j-1)}(\alpha)| \leq \eta$ or $\widetilde{S}^{(j)} = \emptyset$, exit; otherwise increment j by 1.

Return $q^{(j)}(\alpha)$ as an estimate of $q_\chi(\alpha)$.

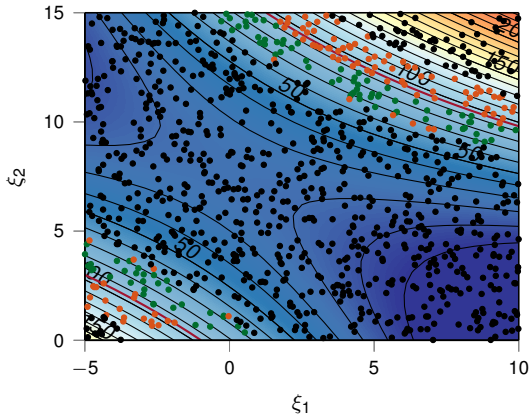

Bifidelity approach: Iterative algorithm

Algorithm Iterative algorithm for the bifidelity method

Initialisation:

1. Build a surrogate model $\widetilde{\chi}$ of χ.
2. Draw ν i.i.d. samples to obtain $S = \left\{\boldsymbol{\xi}(\theta^{(k)}), 1 \leq k \leq \nu\right\}$.
3. Set $k = 0$, $\widetilde{S}^{(0)} = S$, $\Delta\nu \ll \nu$ (step size), and $\eta \geq 0$.
4. Evaluate $\left\{\widetilde{\chi}(\theta^{(k)}), 1 \leq k \leq \nu\right\}$.
5. Set $q^{(0)}(\alpha)$ as the α-quantile of $\left\{\widetilde{\chi}(\theta^{(k)}), 1 \leq k \leq \nu\right\}$.

Iteration: at the j-th iteration ($j \geq 1$), **do**:

1. Sort $\left\{|\widetilde{\chi}(\theta^{(k)}) - q^{(j-1)}(\alpha)|, \theta^{(k)} \in \widetilde{S}^{(j-1)}\right\}$ in ascending order. Let $\Delta\widetilde{S}^{(j)}$ be the $\Delta\nu$ smallest elements and $\widetilde{S}^{(j)} = \widetilde{S}^{(j-1)} \backslash \Delta\widetilde{S}^{(j)}$.
2. Evaluate $\chi(\theta^{(k)})$ and set $\widetilde{\chi}(\theta^{(k)}) = \chi(\theta^{(k)}), \forall \theta^{(k)} \in \Delta\widetilde{S}^{(j)}$.
3. Set $q^{(j)}(\alpha)$ as the α-quantile of $\left\{\widetilde{\chi}(\theta^{(k)}), 1 \leq k \leq \nu\right\}$.
4. If $|q^{(j)}(\alpha) - q^{(j-1)}(\alpha)| \leq \eta$ or $\widetilde{S}^{(j)} = \emptyset$, exit; otherwise increment j by 1.

Return $q^{(j)}(\alpha)$ as an estimate of $q_\chi(\alpha)$.

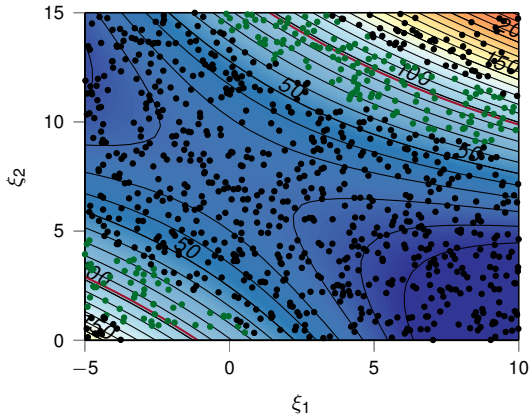

Application: Uncertainty quantification of Antarctic ice-sheet retreat

- Uncertain parameters: Increase in atmospheric temperature after 300 years ($\xi_1 \sim \mathcal{U}[1, 10]$ K) and ratio between the ocean and atmospheric temperature changes ($\xi_2 \sim \mathcal{U}[0.1, 0.9]$).
- Quantity of interest: The grounded portion of the AIS after 700 years.
- Probabilistic representation: We represent the height above floatation as the random field $\{Y(\mathbf{x}), \mathbf{x} \in D\}$ and the grounded portion as the positive random 0-excursion set

$$\mathcal{E}_0^+ = \{\mathbf{x} \in D : Y(\mathbf{x}) \geq 0\}.$$

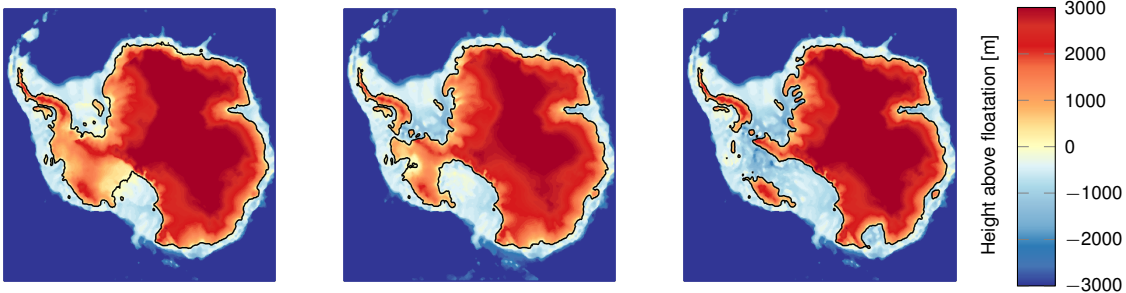

($\xi_1 = 1$ K, $\xi_2 = 0.1$) ($\xi_1 = 5.5$ K, $\xi_2 = 0.5$) ($\xi_1 = 10$ K, $\xi_2 = 0.9$)

Membership functions

- We approximated pointwise probability density functions and statistical descriptors of the random field using a nonintrusive method.
- Membership functions for T_2 and T_3 exhibit a similar behaviour (similar dependence on the coefficient of variation of the random field).
- Larger differences for T_1 are explained by the non-Gaussianity and the bimodality of the random field in vulnerable regions.

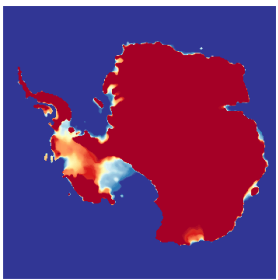

T_1

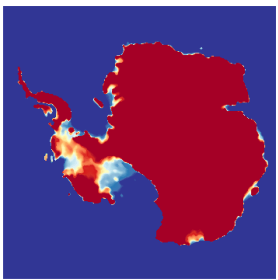

T_2

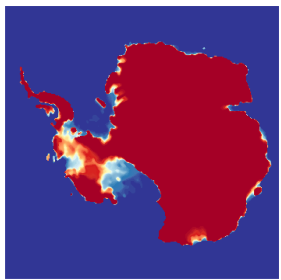

T_3

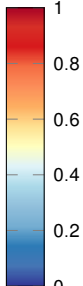

Efficiency of the bifidelity method

- The efficiency of the bifidelity method is measured as the percentage of evaluations of the computational model required to determine a reference quantile (5000 i.i.d. MC samples).
- We observe a speedup of about a factor of 5–10, as compared with the MC reference.
- The efficiency of the bifidelity method is higher for a surrogate model based on a polynomial chaos expansion of χ.
- Comparable efficiency is observed for all three membership functions.

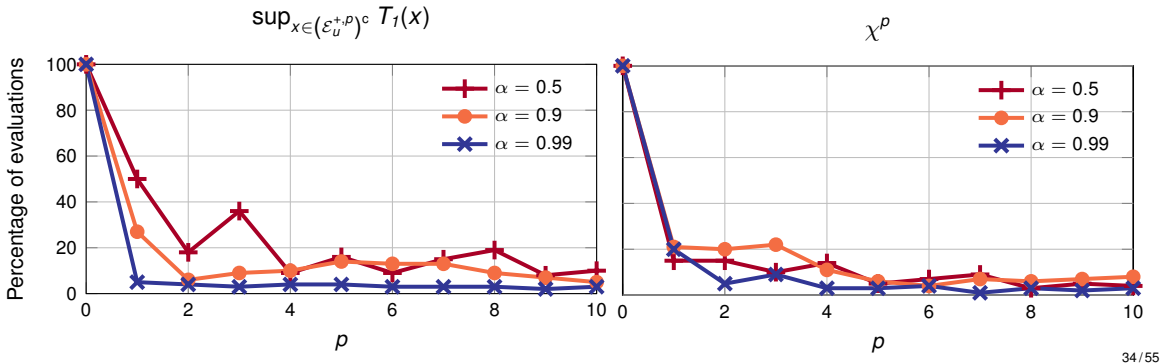

Relationship between the input parameters and HAF/χ^h

- The random variable $Y(\boldsymbol{x}^*)$ ($\boldsymbol{x}^*$ in Siple Coast) has a bimodal distribution with well-separated modes (MISI in Siple Coast). We observe a limited retreat of the grounding line for small forcings and an important retreat for strong forcings.
- The mapping from the values taken by the uncertain input parameters to the value taken by the random variable χ^h is sufficiently smooth to lend itself well to being approximated with low-order polynomial chaos expansions.

$Y(\boldsymbol{x}^*)$ [m]

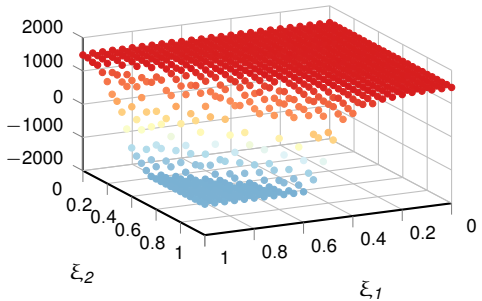

$\chi^h = \max_{i \in (\mathcal{I}_0^{+h})^c} T_1(\boldsymbol{x}_i^h)$

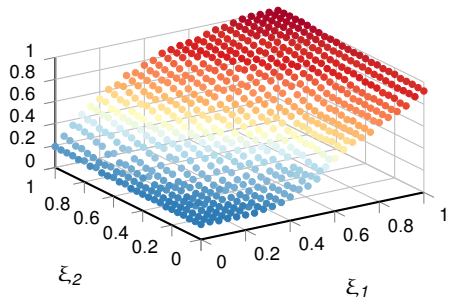

Confidence sets (risk-assessment map)

- We build a risk-assessment map for the retreat of the Antarctic ice sheet by superimposing confidence sets with different levels of probability.
- Confidence sets give insight into the regions most vulnerable to instabilities and the impact of uncertainties on the retreat of the Antarctic ice sheet.
- Confidence sets built on T_2 and T_3 show a higher vulnerability in Amundsen and Filchner sectors than confidence sets built on T_1.

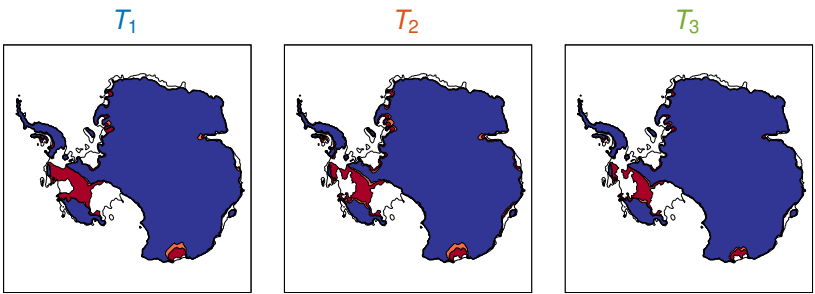

Uncertainty quantification of the multi-centennial response of the Antarctic ice sheet

K. Bulthuis, M. Arnst, S. Sun, and F. Pattyn. Uncertainty quantification of the multi-centennial response of the Antarctic ice sheet to climate change. *Cryosphere*, 13(4), 139-1380, https://doi.org/10.5194/tc-13-1349-2019.

Simulation of the Antarctic ice sheet with f.ETISh

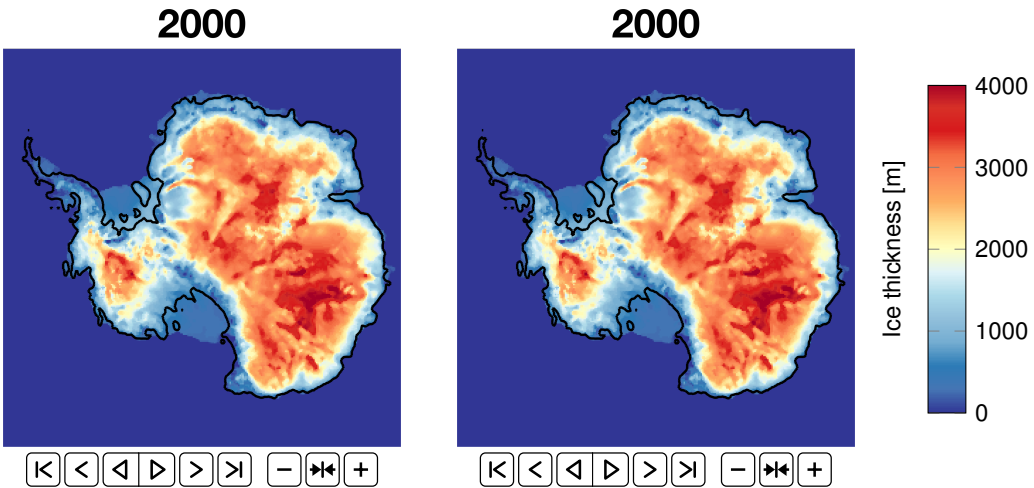

Ice-sheet model and simulations

- Goal: Predicting the response of the AIS over the next millenium with quantified uncertainty (2000–3000 CE).
- Computational ice-sheet model: f.ETISh model (20-km resolution).
- Set of representative scenarios of anthropogenic greenhouse gas emissions (RCP 2.6, RCP 4.5, RCP 6.0, RCP 8.5).

  $\Rightarrow$ Trajectory for change in background atmospheric temperature.
- ΔT acts as a forcing on
  - Temperature and precipitation

$$T = T_0 - \gamma(h - h_0) + \Delta T,$$
$$P = P_0 \times 2^{\Delta T/\delta T};$$

  - Surface melting and refreezing;
  - Ocean temperature and sub-shelf melting

$$T_{\mathrm{oc}} = T_{\mathrm{oc},0} + F_{\mathrm{melt}}\Delta T.$$

- Set of sliding laws defined as characteristic cases of power-law friction $\boldsymbol{v}_{\mathrm{b}} = -A_{\mathrm{b}}\|\boldsymbol{\tau}_{\mathrm{b}}\|^{m-1}\boldsymbol{\tau}_{\mathrm{b}}$ with exponent $m = 1$ (linear), $m = 2$ (weakly nonlinear) and $m = 3$ (strongly nonlinear).
- Grounding-line migration: Schoof's grounding-line flux condition.

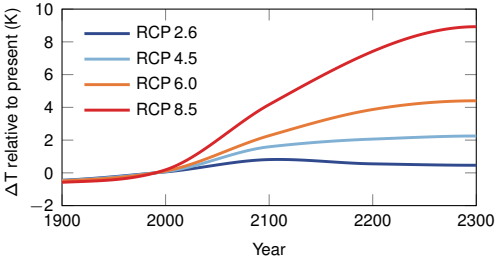

RCP scenarios [Golledge et al., 2015]

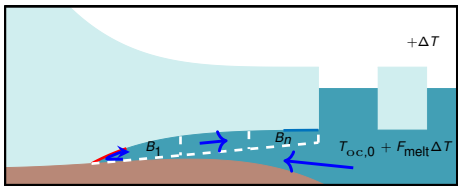

PICO [Reese et al.,2018]

Uncertain parameters and characterisation of uncertainty

$$c_{\mathrm{f}} = F_{\mathrm{calv}} \times c_{\mathrm{f}}^{\#}(h, \mathrm{div}_{\boldsymbol{x}}\mathbf{v})$$

$$F_{\mathrm{calv}} \sim \mathcal{U}(0.5, 1.5)$$

Uncertain calving factor

$$T_{\mathrm{oc}} = T_{\mathrm{oc},0} + F_{\mathrm{melt}}\Delta T$$

$$F_{\mathrm{melt}} \sim \mathcal{U}(0.1, 0.8)$$

Uncertain melt factor

$$\eta = \tfrac{1}{2} E_{\mathrm{shelf}}^{-1} A^{-1/n} \left(\tfrac{1}{\sqrt{2}}\|\boldsymbol{D}\|_{\mathrm{F}}\right)^{\frac{1}{n}-1}$$

$$E_{\mathrm{shelf}} \sim \mathcal{U}(0.2, 1)$$

Uncertain ice-shelf tune factor

$$\frac{\partial b}{\partial t} = -\tfrac{1}{\tau_{\mathrm{a}}}(b - b_0 + w^{\mathrm{eq}})$$

$$\tau_{\mathrm{w}} \sim \mathcal{U}(1000, 3500)\ \mathrm{yrs}$$
$$\tau_{\mathrm{e}} \sim \mathcal{U}(2500, 5000)\ \mathrm{yrs}$$

Uncertain bedrock relaxation times

- In essential ice-sheet models, key processes are represented through parameterisations and reduced-order models with free parameters.
- These are lumped representations of uncertainty. E.g. uncertainty in F_{melt} can represent uncertainties in the shifting of ocean currents, ice-ocean interactions, ...
- Ranges of uncertainty are determined from expert assessment.
- The uncertainty in the sliding law is investigated by considering $m = 1, 2$, and 3.

Uncertain quantification methods

- Quantity of interest: Change in global mean sea level (ΔGMSL) and retreat of grounded ice.
- Propagation of uncertainty:
  - Polynomial chaos expansions (of order 3) as substitutes for the ice-sheet model in the uncertainty quantification (one forward simulation has a computational cost of 8 hours).
  - For each RCP scenario and sliding law: 500 training samples (maximin LHS design).
  - Total CPU time: 48 000 hours.
  - (Embarassingly) parallel computing on Céci clusters.
- Stochastic sensitivity indices:
  - We estimated the Sobol indices from the polynomial chaos coefficients.
- Confidence sets of random excursion sets.

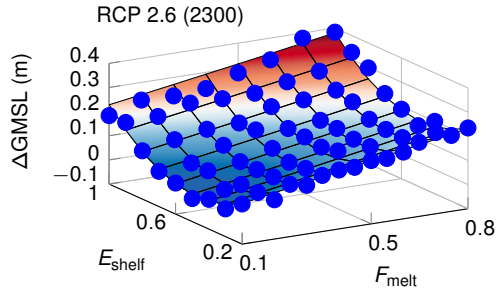

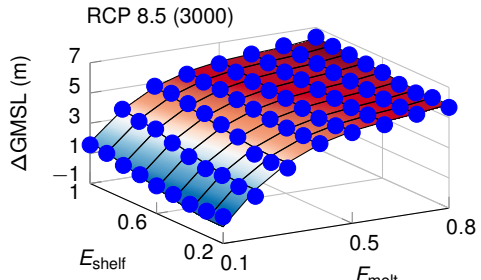

Nominal projections

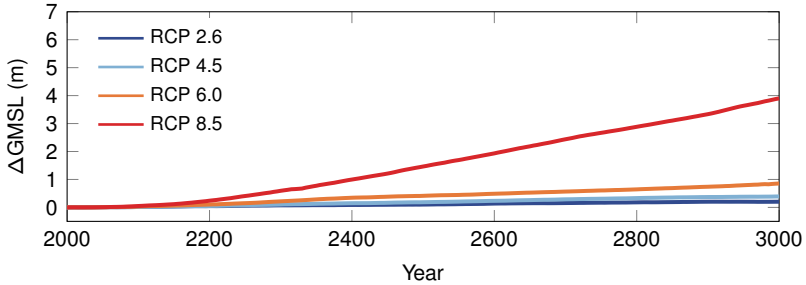

$F_{\text{calv}} = 1$

$F_{\text{melt}} = 0.3$

$E_{\text{shelf}} = 0.5$

$\tau_{\text{w}} = \tau_{\text{e}} = 3000$ yrs

$m = 2$

RCP 2.6

RCP 4.5

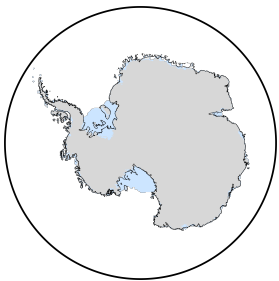

RCP 6.0

RCP 8.5

Parameters-to-projection relationship (RCP 2.6, $m = 2$, 3000 yr)

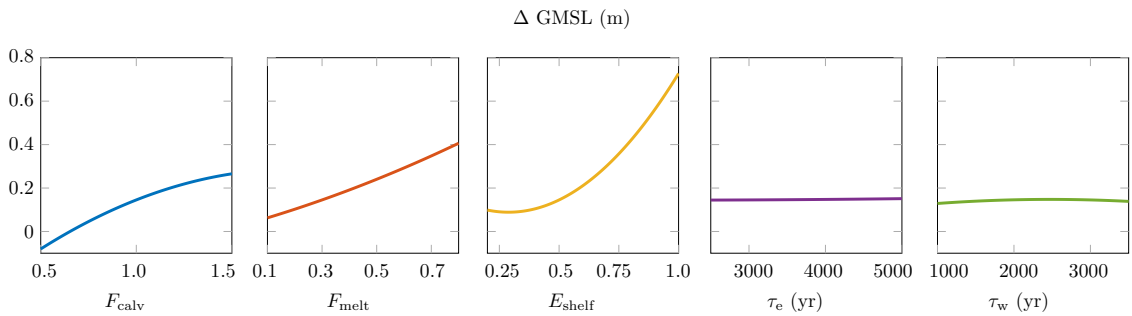

- Nonlinear response with respect to the calving and shelf enhancement factors.
- Linear response with respect to the melt factor.
- The bedrock relaxation times do not contribute significantly to the uncertainty in the projections.

Parameters-to-projection relationship (RCP 8.5, $m = 2$, 3000 yr)

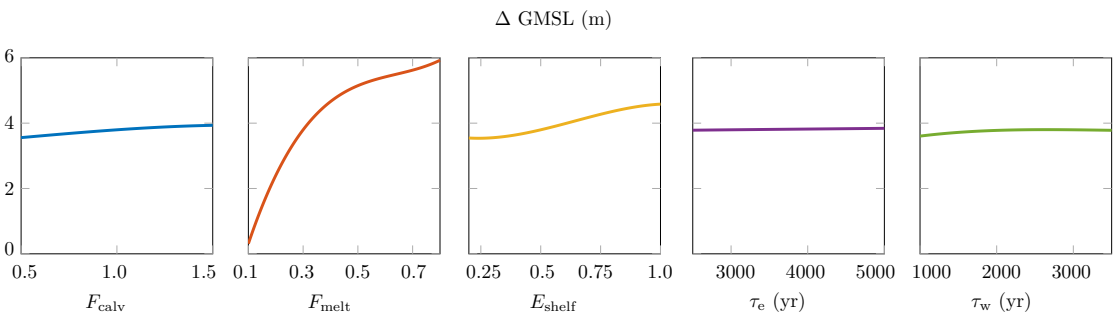

- Nonlinear response with respect with respect to the melt factor. Increasing sub-shelf melting leads to the collapse of the West Antarctic ice sheet. Once the WAIS is disintegrated, a plateau in the response function is reached until marine basins in East Antarctica are activated.
- In the high emission scenario RCP 8.5, the AIS response is controlled by sub-shelf melting.
- The bedrock relaxation times do not contribute significantly to the uncertainty in the projections.

Probabilistic sea-level rise projections ($m = 2$)

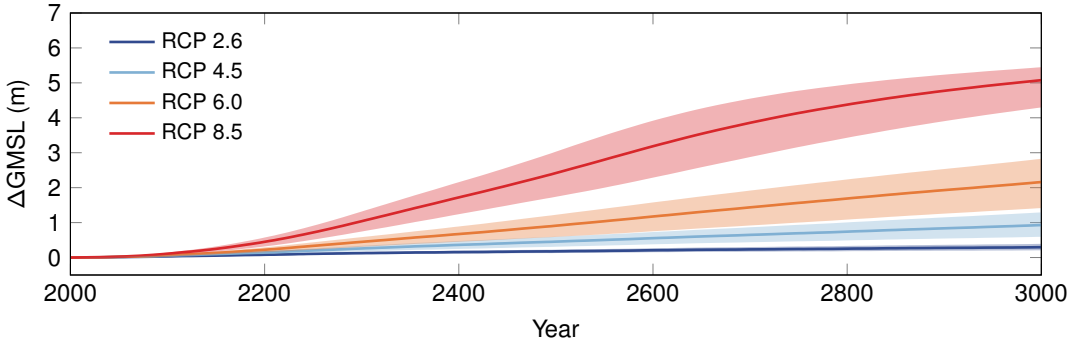

- The AIS contribution to sea level remains limited on short-time scales (2100).
- In warmer scenarios and on longer multi-centennial time scales, the AIS contribution to sea level and the impact of uncertainties on its projection are significant.
- In the strongly mitigated RCP 2.6 scenario, the AIS contribution to sea-level rise remains limited, and this conclusion is robust with respect to the uncertainty.
- More nonlinear sliding conditions favour a more significant ice loss.

Probabilistic sea-level rise projections ($m = 1$)

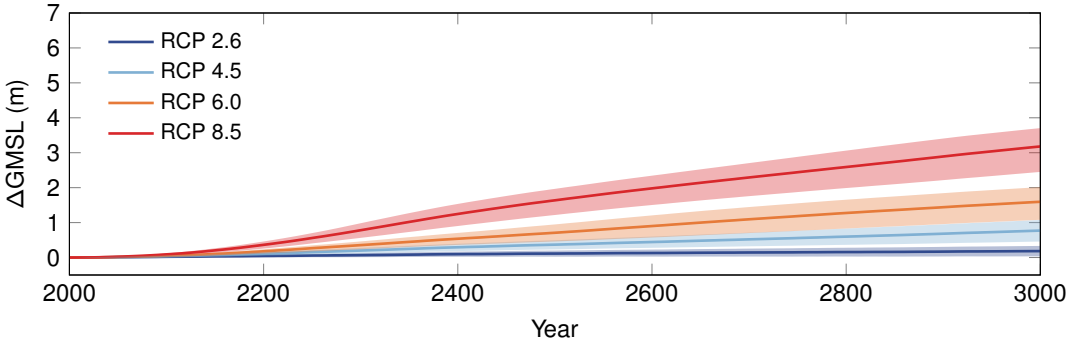

- The AIS contribution to sea level remains limited on short-time scales (2100).
- In warmer scenarios and on longer multi-centennial time scales, the AIS contribution to sea level and the impact of uncertainties on its projection are significant.
- In the strongly mitigated RCP 2.6 scenario, the AIS contribution to sea-level rise remains limited, and this conclusion is robust with respect to the uncertainty.
- More nonlinear sliding conditions favour a more significant ice loss.

Probabilistic sea-level rise projections ($m = 3$)

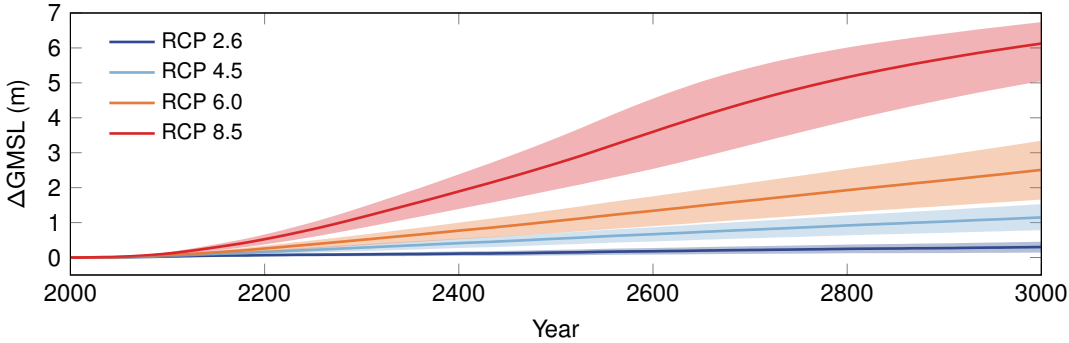

- The AIS contribution to sea level remains limited on short-time scales (2100).
- In warmer scenarios and on longer multi-centennial time scales, the AIS contribution to sea level and the impact of uncertainties on its projection are significant.
- In the strongly mitigated RCP 2.6 scenario, the AIS contribution to sea-level rise remains limited, and this conclusion is robust with respect to the uncertainty.
- More nonlinear sliding conditions favour a more significant ice loss.

Probabilistic sea-level rise projections (probability density)

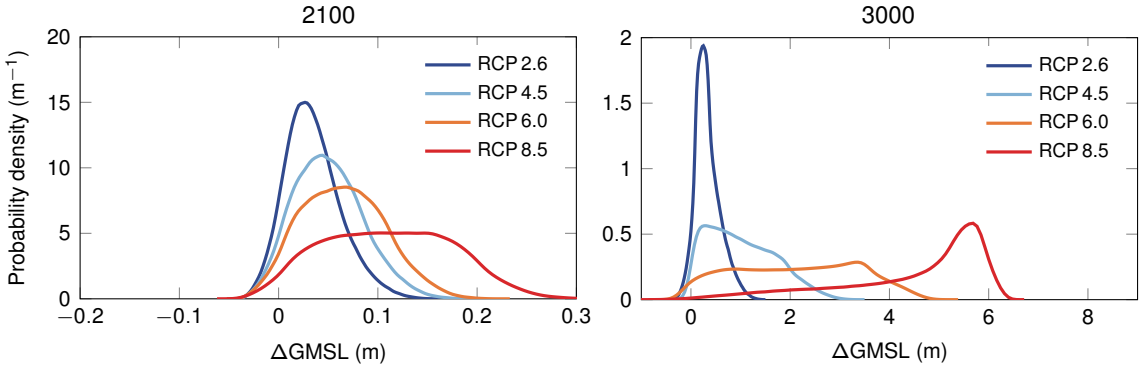

- Unimodal probability densities (wider tails for warmer scenarios and longer timescales).
- RCP 2.6: Gaussian-like distributions.
- RCP 8.5: Rather flat distributions at 2100; More localised mode at higher values at 3000.
- Probability of exceeding 0.5 m by 2100 is negligible (less than 1 %) in all RCP scenarios.
- Probability of exceeding 0.5 m by 3000 in RCP 2.6 is less than 30 %.
- Probability of exceeding 1.5 m by 3000 in RCP 8.5 can reach 95 %.

Probabilistic sea-level rise projections (probability density)

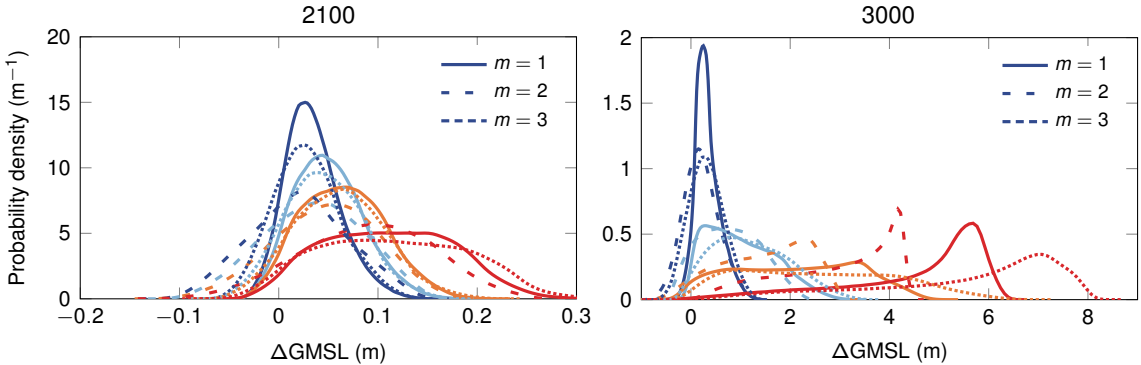

- Unimodal probability densities (wider tails for warmer scenarios and longer timescales).
- RCP 2.6: Gaussian-like distributions.
- RCP 8.5: Rather flat distributions at 2100; More localised mode at higher values at 3000.
- Probability of exceeding 0.5 m by 2100 is negligible (less than 1 %) in all RCP scenarios.
- Probability of exceeding 0.5 m by 3000 in RCP 2.6 is less than 30 %.
- Probability of exceeding 1.5 m by 3000 in RCP 8.5 can reach 95 %.

Sensitivity analysis: Sobol indices

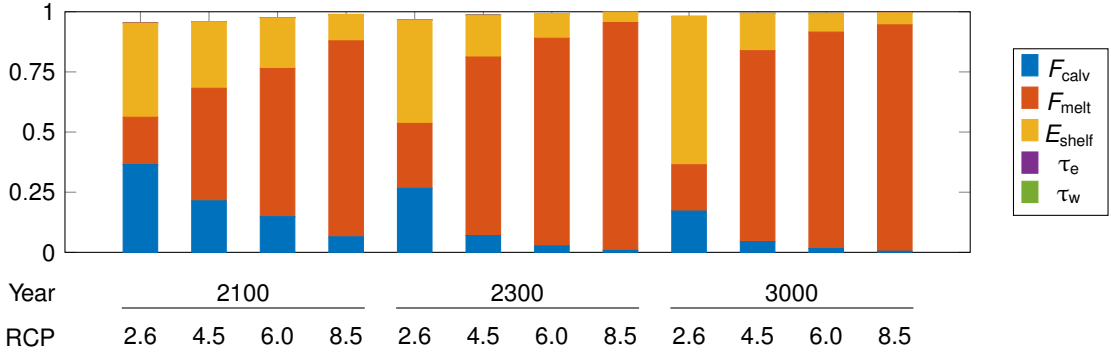

- In the strongly mitigated RCP 2.6 scenario, the dominant source of uncertainty is the uncertainty in ice-shelf rheology followed by those in the calving rate and sub-shelf melting.
- The contribution of the uncertainty in sub-shelf melting to the uncertainty in the projections becomes more and more the dominant source of uncertainty as the scenario gets warmer.
- The bedrock relaxation times do not contribute significantly to the uncertainty in the projections.

Confidence sets ($m = 2$)

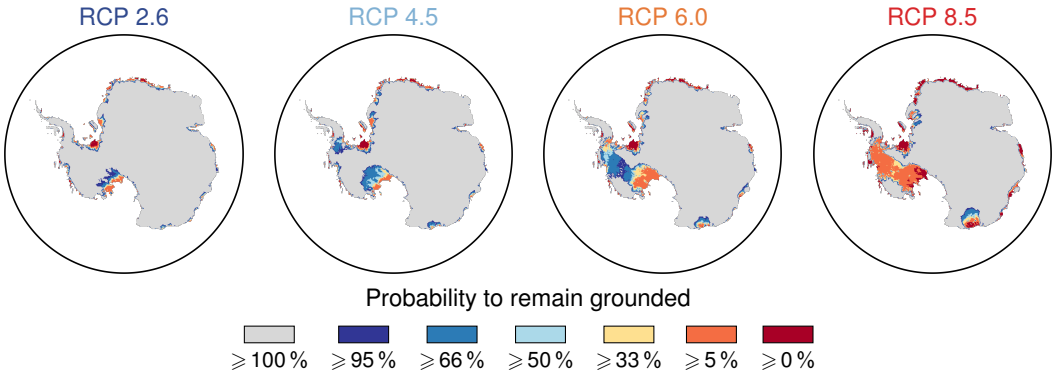

- RCP 2.6: No significant retreat of the grounding line.
- Limited retreat in RCP 4.5 and risk of 33 % of a major collapse of WAIS by 3000 in RCP 6.0.
- RCP 8.5: Risk of 95 % of a major collapse of WAIS by 3000 + Retreat in Wilkes basin.
- In warmer scenarios and for longer timescales, significant mass loss of the AIS is triggered by accelerated retreat of grounded ice in marine sectors.
- More nonlinear sliding conditions favour a more significant ice loss.

Confidence sets ($m = 1$)

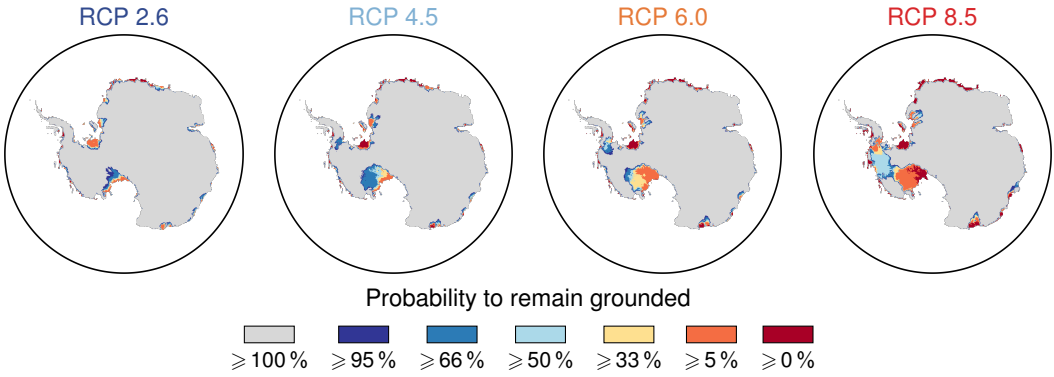

- RCP 2.6: No significant retreat of the grounding line.
- Limited retreat in RCP 4.5 and risk of 33 % of a major collapse of WAIS by 3000 in RCP 6.0.
- RCP 8.5: Risk of 95 % of a major collapse of WAIS by 3000 + Retreat in Wilkes basin.
- In warmer scenarios and longer timscales, significant mass loss of the AIS is triggered by accelerated retreat of grounded ice in marine sectors.
- More nonlinear sliding conditions favour a more significant ice loss.

Confidence sets ($m = 3$)

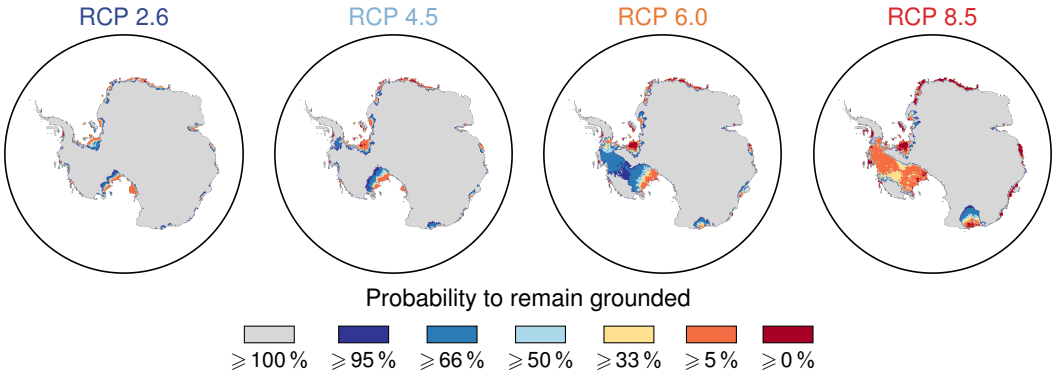

- RCP 2.6: No significant retreat of the grounding line.
- Limited retreat in RCP 4.5 and risk of 33 % of a major collapse of WAIS by 3000 in RCP 6.0.
- RCP 8.5: Risk of 95 % of a major collapse of WAIS by 3000 + Retreat in Wilkes basin.
- In warmer scenarios and longer timscales, significant mass loss of the AIS is triggered by accelerated retreat of grounded ice in marine sectors.
- More nonlinear sliding conditions favour a more significant ice loss.

Probabilistic sea-level rise projections ($m = 2$ + TGL)

- TGL parameterisation exhibits an increased grounding-line sensitivity to environmental changes.
- Probability of exceeding 0.5 m by 2100 is still negligible (less than 1 %) in all RCP scenarios.
- RCP 2.6: Probability of exceeding 0.5 m and 1 m by 3000 can reach more than 40 % and 10 %, respectively.
- Faster and more significant grounding-line retreat in marine sectors and additional mass loss from East Antarctica, especially in the Aurora basin.

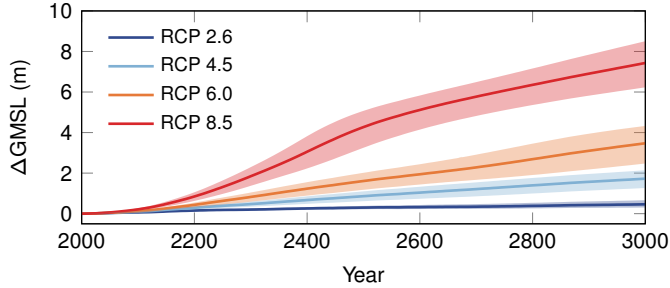

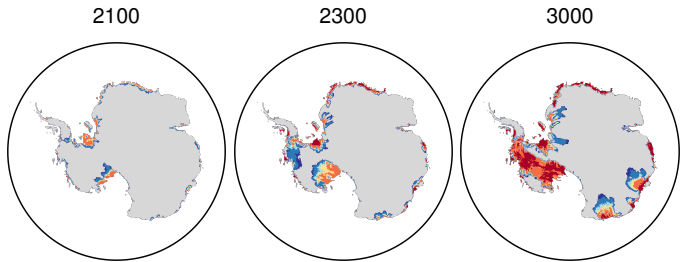

Uncertainty quantification of the AIS response: Discussion

- Comparison of the sea-level rise projections:
  - RCP 2.6: Projections in agreement with Golledge et al. (2015) and DeConto and Pollard (2016) by 2100.
  - RCP 8.5: Projections in agreement with Golledge et al. (2015) but less important than in DeConto and Pollard (2016).
- Comparison of grounded-ice retreat:
  - Grounding-line retreat is the most significant in the Siple Coast (idem Golledge et al., 2015).
  - Grounding-line retreat is less sensitive in the Amundsen Sea sector than in Cornford et al. (2015), Ritz et al. (2015), and Schlegel et al. (2018).
- Impact of parametric uncertainty on AIS projections:
  - The significance of the response of the AIS is controlled by the sensitivity, the response time and the vulnerability of marine drainage basins. The threshold for instability can be reached through various combinations of the parameters;
  - RCP 2.6: Projections are robust under parametric uncertainty (no collapse of AIS);
  - RCP 4.5, 6.0: Projections are sensitive to parametric uncertainty;
  - RCP 8.5: Projections are robust under parametric uncertainty (complete collapse of WAIS).

Multi-model comparison of sea-level rise projections

Multi-model comparison (2100)

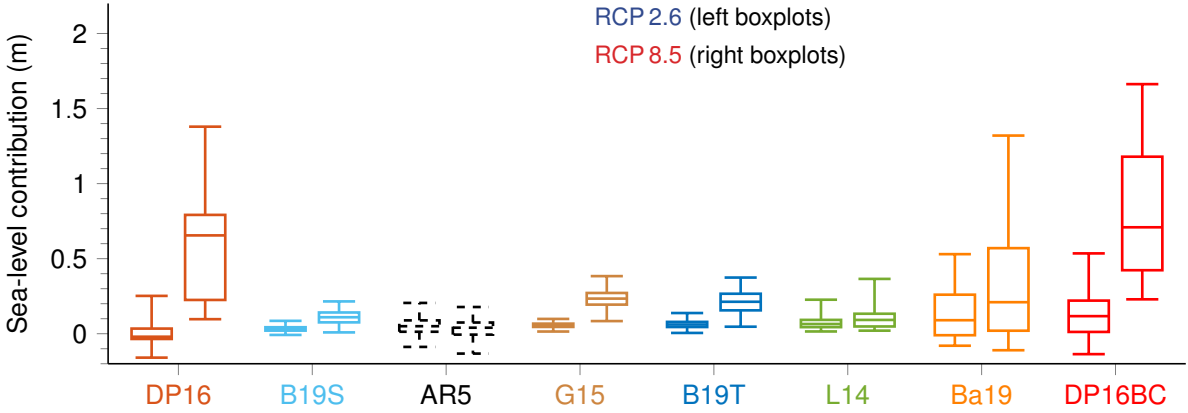

- RCP 2.6: All models agree on a limited median contribution to sea-level rise (below 0.2 m). 95 % percentiles are below 0.5 m for most models.
- RCP 8.5: Median contribution is 0.04–0.23 m without MICI but can reach 0.66 m with MICI. 95 % percentiles are below 0.5 m for most models without MICI but exceed 1 m with MICI.
- Ice-sheet dynamical changes dominate increased snowfall (in contrast with AR5).

Multi-model comparison (2300)

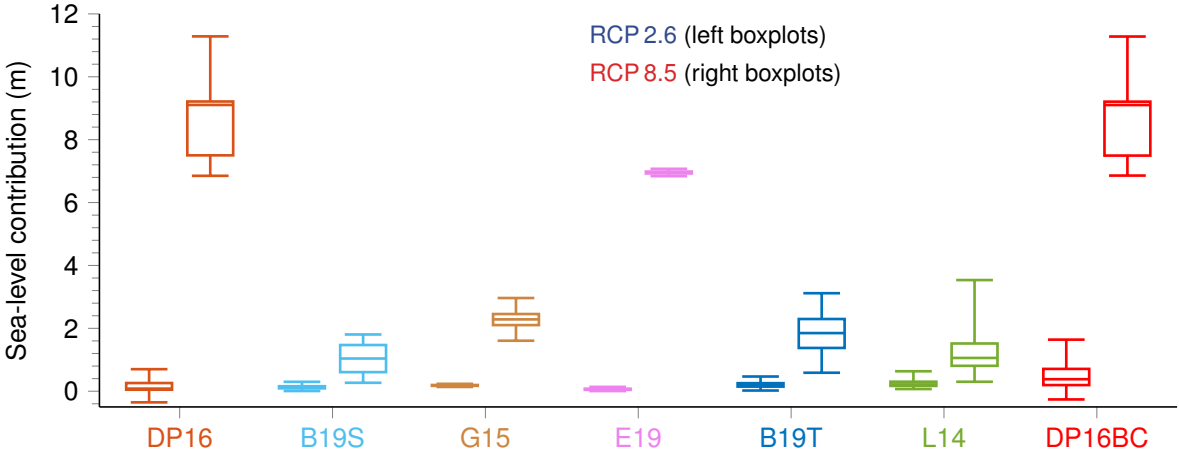

- Deep uncertainty in projections beyond 2100 (only a limited number of studies).
- RCP 2.6: Most models agree on a median contribution below 0.5 m.
- RCP 8.5: All models agree on a median contribution above 1 m but large differences in the magnitude of the contribution between models with and without MICI.

Conclusion and outlook

Conclusion and outlook

- We contributed to clarifying the role played by uncertainties in the continental response of the Antarctic ice sheet to climate change on multicentennial-to-millenial timescales.
  - New insight into the impact of uncertain input parameters on the AIS contribution to sea-level: We provided new probabilistic projections of sea-level rise (used in SROCC [2019]), we carried out a sensitivity analysis to identify the most influential sources of uncertainty, and drew risk-assessment maps to identify regions most vulnerable to instabilities.
  - Contribution to UQ of geometrical characteristics of the spatial response of physics-based computational models : We proposed a new efficient bifidelity method for the estimation of confidence sets of random excursion sets and used these confidence sets to quantify with uncertainty the retreat of the grounded portion of the AIS.
- Directions for future research:
  - Improvement in initialisation schemes, ice-sheet coupling with other Earth system components, and numerical methods for the migration of the grounding line.
  - Improved datasets (ocean conditions, bedrock topography,...).
  - Advanced UQ methods (e.g. PLoM, multifidelity methods, ensemble propagation,...).
  - Improvement of probabilistic characterisation of uncertainty in ice-sheet models (information theory, Bayesian inference,...).
  - Methods to quantify the impact of model uncertainties in ice-sheet models.
  - Impact of stochastic perturbations on the stability of ice sheets.

Acknowledgement

The author, Kevin Bulthuis, would like to acknowledge the Belgian National Fund for Scientific Research (F.R.S.-FNRS) for its financial support (F.R.S.-FNRS Research Fellowship).

Towards robust prediction of the dynamics of the Antarctic ice sheet

Uncertainty quantification of sea-level rise projections and grounding-line retreat with essential ice-sheet models

Kevin Bulthuis[1,2]

[1] Computational and Stochastic Modeling, Université de Liège, Belgium
[2]Laboratory of Glaciology, Université Libre de Bruxelles, Belgium